Structure and dynamics of human perilipin 3 membrane association

Yong Mi Choi[1a], Dalila Ajjaji[2a], Kaelin D. Fleming[3], Peter P. Borbat[5,6], Meredith L. Jenkins[3], Brandon E Moeller[3], Jack H. Freed[5,6], John E. Burke[3,4*], Abdou Rachid Thiam[2*], Michael V. Airola[1*]

[1]Department of Biochemistry and Cell Biology, Stony Brook University, Stony Brook NY 11794, USA

[2]Laboratoire de Physique de l'École normale supérieure, ENS, Université PSL, CNRS, Sorbonne Université, Université Paris Cité, F-75005 Paris, France

[3]Department of Biochemistry and Microbiology, University of Victoria, Victoria BC V8N 1A1, Canada

[4]Department of Biochemistry and Molecular Biology, The University of British Columbia, Vancouver, British Columbia V6T 1Z3, Canada

[5]National Biomedical Center for Advanced Electron Spin Resonance Technology, Cornell University, Ithaca, United States

[6]Department of Chemistry and Chemical Biology, Cornell University, Ithaca, United States

*Address correspondence to:

Michael V. Airola, michael.airola@stonybrook.edu

Abdou Rachid Thiam, thiam@ens.fr

John E. Burke, jeburke@uvic.ca

ABSTRACT

Lipid droplets (LDs) are dynamic organelles that contain an oil core mainly composed of triglycerides (TAG) that is surrounded by a phospholipid monolayer and LD-associated proteins called perilipins (PLINs). During LD biogenesis, perilipin 3 (PLIN3) is recruited to nascent LDs as they emerge from the endoplasmic reticulum. Here, we analyzed how lipid composition affects PLIN3 recruitment to membrane bilayers and LDs, and the structural changes that occur upon membrane binding. We found the TAG precursors phosphatidic acid and diacylglycerol (DAG) recruit PLIN3 to membrane bilayers and define an expanded PAT domain that preferentially binds DAG enriched membranes. Membrane binding induces a disorder/order transition of alpha helices within the PAT domain and 11-mer repeats, with intramolecular distance measurements consistent with the expanded PAT domain adopting a triangular tertiary structure. In cells, PLIN3 is recruited to DAG enriched ER membranes, and this requires both the PAT domain and 11-mer repeats. This provides molecular details of PLIN3 recruitment to nascent LDs and identifies a function of the PAT domain of PLIN3 in DAG binding.

INTRODUCTION

Lipid droplets (LDs) act as energy reservoirs in cells. They contain a neutral lipid core of mainly triacylglycerides (TAGs) and cholesterol esters with a phospholipid monolayer that surrounds the neutral lipid core. This creates a membrane environment for LDs that is distinct from membrane bilayers and recruits several LD-associated proteins [1-3]. In addition to a major role in energy storage, LDs are also important cellular hubs that traffic proteins and lipids between organelles, regulate ER stress, and contribute to viral infections [4-6].

LDs are formed in the ER where neutral lipids are synthesized [7, 8]. Mechanistically, LD formation involves several steps [9] including accumulation of neutral lipids in the outer ER membrane leaflet, neutral lipid nucleation aided by the Seipin complex and associated factors (e.g. LDAF1) [10], formation of nascent LDs that bud from the ER [11, 12] and LD growth and maturation [13, 14]. Several lines of evidence support the idea that the phospholipid composition of the ER membrane is locally edited to promote LD assembly or recruit specific proteins important for LD formation such as seipin and ORP proteins [7, 15-17]. Although there is still uncertainty regarding the phospholipid composition at the initial stages of LD formation, evidence from yeast suggest diacylglycerol (DAG), the direct precursor of TAG, is enriched in discrete ER subdomains where LD biogenesis is initiated [15, 18]. DAG can also promote TAG nucleation and impact the architecture of LDs on the ER [15, 19].

Perilipins (PLINs) are the major class of proteins that coat the surface of LDs [20-26]. There are five PLINs in humans that bind LDs at various stages of their initiation and maturation [21]. For example, PLIN1 is the major PLIN that binds to mature LDs in adipocytes, while PLIN2 and PLIN5 reside on mature LDs in liver and muscle cells, respectively [27]. In contrast, PLIN3 displays near ubiquitous expression and binds to early LDs as they bud from the ER, but is later displaced by other PLINs as LDs grow and mature [10, 28]. PLIN3 is unique in that it is stable and not degraded in the absence of LDs. This allows PLIN3 to translocate from the cytoplasm to sites of early LD formation, where it acts as a marker for the biogenesis of early LDs [10, 28-33].

PLINs share a conserved protein domain architecture composed of an N-terminal PAT domain, followed by variable stretches of 11-mer repeats and a C-terminal 4-helix bundle [34, 35]. The 11mer repeats form amphipathic helixes that are sufficient to recruit PLINs to LDs [34-36], while the 4-helix bundle in some PLINs can also bind LDs [34, 37]. Although the PAT domain is the

most conserved domain among PLINs, its function is not clear, as it has not been demonstrated to bind to membranes or LDs.

Here, we examined the mechanism of PLIN3 recruitment to membrane bilayers and LDs using a combination of *in vitro* and cell culture assays, and analyze the structural changes induced by membrane binding using hydrogen-deuterium exchange mass spectrometry (HDX-MS) and pulsed-dipolar electron spin resonance spectroscopy (PD-ESR). We found that human PLIN3 is recruited to membrane bilayers enriched in the TAG precursors phosphatidic acid (PA) and DAG. By delineating the roles of the PAT domain and 11-mer repeats, we define an expanded PAT domain that is sufficient for PLIN3 to bind DAG enriched membranes, while the 11-mer repeats are sufficient to bind LD monolayers. We confirm that DAG enrichment can drive PLIN3 recruitment to ER membranes in cells, and this requires both the PAT domain and 11-mer repeats. Structurally, the PAT domain and 11-mer repeats form inducible alpha helices to drive membrane association and the PAT domain forms a tertiary structure upon membrane binding. Taken together, this study provides molecular insight into how PLIN3 is recruited to early LDs and reveals a novel function for the PAT domain of PLIN3 in DAG binding.

RESULTS

The Triglyceride Precursors DAG and PA Recruit PLIN3 to Membrane Bilayers

To systematically define how lipid composition affects PLIN3 recruitment to membrane bilayers, we purified recombinant human PLIN3 from *Escherichia coli* and used liposome co-sedimentation assays to monitor membrane binding. Liposomes were prepared from phospholipids with different acyl-chain combinations comprised of either palmitoyl-oleoyl (PO) or di-oleoyl (DO) phospholipids **(Fig. 1A)**. PO phospholipids have one unsaturated acyl chain and are representative of the typical lipid composition in ER membranes. DO phospholipids contain two unsaturated acyl chains, have increased membrane packing defects [38] and are enriched in ER membranes after oleate supplementation, which stimulates LD formation [15, 39-41]. Initial liposome co-sedimentation experiments varied the ratio of neutral phospholipids phosphatidylcholine (PC) and phosphatidylethanolamine (PE), as PC and PE represent the major lipids on both the cytoplasmic face of the endoplasmic reticulum (ER) and surface of LDs, and the ratio of PC to PE has previously been shown to regulate protein distribution on LDs [42]. Under all PC to PE ratios tested, PLIN3 did not bind liposomes comprised solely of PC and PE **(Fig. 1B)**.

We next asked whether addition of other lipids that are synthesized in the ER could recruit PLIN3 to membranes by generating PC/PE liposomes containing 20 mol% of either phosphatidic acid (PA), phosphatidylserine (PS), diacylglycerol (DAG), phosphatidylinositol (PI) or C18:1 ceramide. Regardless of lipid composition, PLIN3 did not bind to any PO-based liposomes **(Fig. 1C, 1D)**. However, PLIN3 was recruited to DO-based liposomes enriched in DAG or PA **(Fig. 1C, 1D)**. Addition of DOPS and ceramide resulted in a minor increase in PLIN3 binding in DO-based liposomes, while the addition of PI had no effect **(Fig. 1C, 1D)**.

PLIN3 recruitment to DO-based liposomes depended on the surface concentration of DAG, with 5 mol% DAG able to induce ~10% binding, and 20 mol% DAG inducing 35% binding **(Fig. 1E)**. The addition of DOPA further increased PLIN3 binding in DAG-containing liposomes, which suggested a synergistic effect of PA and DAG on PLIN3 membrane recruitment **(Fig. 1F)**. Increasing the total liposome concentration caused the majority of PLIN3 to bind membranes, but 10% of PLIN3 remained in the soluble fraction **(Fig. S1A)**. We concluded that PLIN3 is recruited to liposomes containing DAG and/or PA, which are notably the membrane-lipid precursors for triglyceride synthesis.

PLIN3 Binds to Liposomes with Membrane Packing Defects

LDs have increased membrane packing defects in comparison to membrane bilayers. Previously, PLIN4 has been shown to have increased binding to liposomes composed of methyl branched diphytanoyl (4ME) phospholipids that create shallow lipid-packing defects that can be accessed by hydrophobic insertion of peripheral membrane proteins, such as PLINs [35, 43]. As a comparison to DO and PO liposomes, we found 4ME phospholipids significantly increased PLIN3 liposome association with ~70% binding observed with a mixture of 4ME-PC and 4ME-PE **(Fig. 1G)**. Consistent with our previous observations, 4ME-PA further increased PLIN3 binding, while 4ME-PS and C18:1 ceramide decreased binding **(Fig. 1G)**. The effect of 4ME-DAG was unable to be assessed as addition of 4ME-DAG disrupted proper liposome formation. Taken together, this suggests PLIN3 also binds membranes with lipid packing defects, which can be further enhanced by PA.

PLIN3 Binding to Artificial Lipid Droplets

As the major function of PLIN3 is to bind to emerging LDs as they bud from the ER, we next assessed the ability of recombinant PLIN3 to bind artificial lipid droplets (ALDs) *in vitro* using a flotation assay [10, 28, 44, 45]. ALDs were generated with a triolein neutral lipid core surrounded by a phospholipid monolayer of DOPC and DOPE in 1:2.5 molar ratio of phospholipids to TAG. ALDs with 80 mol% DOPC and 20 mol% DOPE showed 50% binding of PLIN3 **(Fig. S1B)**. The addition of the anionic phospholipids PI4P decreased PLIN3 binding to ALDs. In contrast, PA, PS and PI slightly decreased binding, ceramide did not affect binding, and DAG slightly increased PLIN3 binding. However, none of these effects were statistically significant. The modest impact of these PA, PS, PI, DAG, and ceramide, which all can induce negative curvature or charge in membrane bilayers, may be due to the basal occurrence of significant phospholipid packing voids on the ALD surface as compared with bilayers; while the strongly charged PI4P would instead mask these and diminish binding [46].

The PAT Domain and 11-mer Repeats are Disordered in the Absence of Membranes

We next sought to examine how the structure of PLIN3 changes upon membrane binding, first focusing on the structure of PLIN3 in the absence of membranes. For these experiments, we used hydrogen deuterium exchange mass spectrometry (HDX-MS), which measures the exchange of amide hydrogens with deuterated solvent, which acts as a readout for protein conformational

dynamics of secondary structure [47, 48]. A brief pulse of deuterated solvent is useful for identifying regions within a protein that lack structure compared to ordered regions [49, 50].

We determined the absolute exchange of PLIN3 after a 3 sec pulse of deuterium incorporation at 1°C (equivalent to ~0.3 s at 18°C) using a fully deuterated control. After the deuterium pulse, the first 200 residues of PLIN3 comprising the PAT domain and 11-mer repeats were fully deuterated, indicating these regions are completely disordered in the absence of membranes **(Fig. 2A)**. The 4-helix bundle and a/b domain were largely ordered with comparatively low rates of deuterium incorporation **(Fig. 2A)**, which is consistent with the crystal structure of mouse PLIN3 (previously referred to as Tip47) [51].

The PAT Domain and 11-mer Repeats are the Major Drivers of PLIN3 Membrane Association

We next sought to determine any conformational changes that occur during membrane binding using HDX-MS. Having established optimal conditions for PLIN3 membrane binding, we measured the deuterium exchange rate over various time points (3, 30, 300, and 3000 sec) in the absence or presence of 4ME liposomes composed of 60 mol% 4ME-PC, 20 mol% 4ME-PE, and 20 mol% 4ME-PA.

In the presence of membranes, striking differences in deuterium exchange were observed throughout the PLIN3 sequence **(Fig. 2E, Table S1, source data)**. The most notable differences were large decreases in deuterium exchange in the PAT domain and 11-mer repeat regions. In comparison to previous results that demonstrated the 11-mer repeats are sufficient for lipid droplet association [34, 35], this suggests that the PAT domain and 11-mer repeats are both major contributors to membrane binding. Consistently, we found that a purified fragment of the PAT domain and 11-mer repeats displayed similar membrane recruitment as full-length PLIN3 to DO liposomes enriched in DAG and PA, and 4ME liposomes **(Fig. 2C, 2D)**.

The HDX-MS results suggested that membrane-binding induces the formation of secondary structure in the PAT domain and 11-mer repeats. This is consistent with both alpha fold and RoseTTA fold models that predict the PAT domain and 11-mer repeats form amphipathic alpha helices, with the PAT domain adopting a triangular globular structure and the 11-mer repeats

forming a series of extended alpha helices **(Fig. 2B, 3B)**. Based on these results we concluded that the PAT domain and 11-mer repeats of PLIN3 are intrinsically disordered in the absence of membranes, with inducible amphipathic alpha helices being stabilized upon membrane binding.

Notably, many of the peptides with the PAT domain and 11-mer repeats displayed a bimodal distribution of deuterium exchange upon membrane binding **(Fig. S2A, S2B)**. This differs from a canonical distribution where the degree of deuteriation is gaussian in individual peptides. The observed bimodal distributions are consistent with either EX1 exchange [52], or there being two distinct protein conformations in the sample. Depending on the membrane residency of PLIN3, bimodal distributions can be consistent with observations of the free and membrane bound state. Given our previous observation that the PAT and 11-mer repeats are intrinsically disordered in the absence of membranes, the simplest interpretation is that the PAT domain and 11-mer repeats cycle between two states: 1) a membrane bound alpha helical state on membranes that is strongly protected from H-D exchange and 2) an intrinsically disordered solution state that rapidly exchanges with deuterated solvent upon dissociation from membranes and leads to rapid H-D exchange. Therefore, the half-life of bimodal exchange can act as a surrogate for membrane residency time for disordered regions of the protein.

The protection from deuterium exchange and the non-gaussian bimodal distribution for most peptides in the PAT domain persisted over a longer time course (~300 sec) in comparison to peptides within the 11-mer repeat regions (~30 sec) **(Fig. S3A)**. This trend of longer HDX protection correlated with the degree of sequence conservation among PLINs **(Fig. 3A)**. Taken together this supports a role for the PAT domain in membrane binding and suggests a similar role for the highly conserved PAT domain in other PLINs.

In contrast to the N-terminal PAT domain and 11-mer repeats, the C-terminal 4-helix bundle displayed a large increase in deuterium exchange **(Fig. 2E, S3A)**. The most apparent increase in deuterium exchange was in the middle of the 4-helix bundle (residues 230-270). We hypothesized this was due to the 4-helix bundle unfolding upon membrane binding, with this possibly contributing to membrane recruitment **(Fig. S3A)**. To test this, we examined the ability of a purified PLIN3 4-helix bundle fragment (residues 197-427) to bind membranes. Consistent with our hypotheses, the isolated 4-helix bundle bound to the 4ME-PC/PE/PA liposomes that were used in the HDX-MS experiment **(Fig. 2C, 2D)**. However, the 4-helix bundle did not bind to

4MEliposomes lacking PA, or to any DO-based liposomes even when PA and DAG were present **(Fig. 2C, 2D)**. We concluded that the 4-helix bundle of PLIN3 can unfold and bind membranes, but only under these specific lipid compositions that induce severe membrane packing defects and in the presence of PA.

To understand how lipid composition influences the structure of PLIN3 we again applied HDXMS, using variable liposome compositions of 4ME-PC/PE and DOPC/PE/DAG **(Fig. 2F, 2G)**. In line with of previous HDX-MS and liposome sedimentation experiments, we observed protection from H-D exchange in the PAT domain and 11-mer repeats using 4ME-PC/PE and DOPC/PE/DAG liposomes, with the magnitude and duration of H-D exchange protection in these regions correlating with the observed fraction of PLIN3 bound in liposome sedimentation assays **(Fig. S3B, 1D and 1G)**.

In contrast, with the 4ME-PC/PE and DOPC/PE/DAG lipid compositions, the 4-helix bundle did not display large increases in deuterium exchange indicating that 4-helix bundle is not involved in membrane binding in the absence of PA. Taken together, these results confirm that the PAT domain and 11-mer repeats are the major lipid interacting regions of PLIN3, and that the 4-helix bundle forms a stable tertiary structure that in general does not contribute to membrane association, unless PA is present.

An expanded PAT domain binds DAG enriched membranes

Our results suggested a role for the PAT domain in PLIN3 membrane association. However, several studies [34, 35] have previously established the 11-mer repeats of PLINs are sufficient for membrane binding, and to our knowledge, the PAT domain alone has not been demonstrated to bind membranes. Complicating matters, the precise boundaries of the PAT domain have been difficult to establish. Previous studies have suggested the PAT domain consists of the N-terminal 97 residues in PLIN3 [34], which are highly conserved with other PLINs **(Fig. 3A)**. However, high sequence conservation between PLINs continues beyond residue 97 and ends at residue 115 in PLIN3 **(Fig. 3A)**. This suggests the PAT domain may be larger than previously expected. Consistent with the sequence conservation, both Alphafold [53] and RoseTTA fold [54] predict a triangular alpha helical tertiary structure for the PAT domain that encompasses residues 22-115 **(Fig. 3B)**.

To investigate the PAT domain boundaries and membrane interaction capabilities, we purified several C-terminal extended PAT domain constructs and the corresponding 11-mer repeats counterparts **(Fig. 3C)** and assessed the ability of these fragments to bind DO-liposomes containing either 20 mol% PA or 20 mol% DAG. As an important note, we were unable to purify the previously suggested PAT domain construct (residues 1-97), as this construct was not stably expressed in *Escherichia coli*. This is consistent with the poor expression of the PAT domain of PLIN1 in yeast [34].

In general, fragments encompassing the PAT domain bound strongly to liposomes in the presence of DAG, with modest liposome binding in the presence of PA **(Fig. 3D)**. In contrast, the 11-mer repeats bound to liposomes containing either PA or DAG **(Fig. 3D)**. While the exact boundaries of the PAT domain and 11-mer repeats remain difficult to precisely define, this suggests an expanded PAT domain is capable of membrane binding and displays a preference for binding DAG enriched membranes, while the 11-mer repeats of PLIN3 do not.

Conformational Rearrangements of the PAT Domain upon Membrane Binding

We next sought to determine if membranes induced conformational changes in the PAT domain consistent with the structures predicted by Alphafold and RoseTTAfold. To monitor conformational changes, we applied the pulsed-dipolar spectroscopy (PDS) technique of double electronelectron resonance (DEER) [55, 56] to full-length PLIN3 in solution and bound to liposomes. PDS is a collection of several, based on recording electron spin-echo (ESE), pulse ESR techniques [57-61] routinely applied to characterize protein conformations by providing accurate constraints in the distance range of ~10-90 Å. The amplitude of detected ESE depends on dipolar coupling between the spins of unpaired electrons in nitroxide spin labels covalently bound to engineered cysteine residues. Stepping out pulse separation in the sequence produces the time domain ESE envelope, from which the distances could be reconstructed. [57-60].

Two sets of residues (25 and 96; 37 and 114) were selected for spin labeling, which were respectively 71 and 77 residues apart in the primary sequence but predicted to be in close proximity by AlphaFold and RosettaFold **(Fig. 4A)**. Comparison of the DEER decoherence (decay) times indicated that the PAT domain is less structured and/or intrinsically disordered in solution versus when bound to liposomes, which is consistent with our HDX-MS analysis **(Fig. 4B, 4C)**. In liposomes the decoherence times are fast enough to decay to background well within the evolution

time of 1.2 μs used in the liposome DEER measurements. They do not show oscillations, which is frequently observed for membrane proteins. [62-65]. As a control to rule out lateral aggregation [63], we attached a single spin-label to residue 37C and did not observe a dipolar evolution (DEER shape) that could indicate a pair with a shorter than ~80 Å separation based on only slightly concave shape of the signal **(Fig. 4D)**. The DEER data thus suggest that conspicuous dipolar signals in the doubly labeled proteins result from intramolecular interactions, rather than being caused by intermolecular interactions on membranes.

Distance distributions could be obtained in the presence of liposomes. The results showed semibroad distance spreads of ~20-40Å for the 25C/96C pair and ~20-35Å for the 37C/114C pair **(Fig. 4E, 4F)**. These distances are comparable but do not exactly match the simulated distances using the AlphaFold and RoseTTAfold structure predictions [53, 54]. For comparison, an extended alpha helix would result in distances of ~100Å for these two sites. We also checked the spectral shape by recording field-swept echo and did not notice any broadening that could indicate a shorter range of distances (<15 Â) to which employed DEER sequence is not sensitive. Taken together, we concluded that the PAT domain does form a folded domain when bound to membranes and this domain is likely mobile with a structure similar but not identical to the AlphaFold and RoseTTAfold predictions.

DAG recruits PLIN3 to membrane bilayers and droplets in vitro

To verify a role for the PAT domain in DAG binding, we conducted an independent set of experiments to test if purified PLIN3 with GFP fused to the N-terminus bound DAG-enriched membranes using droplet embedded vesicles (DEVs) [7, 42, 66, 67]. DEVs have emerged as a powerful in vitro system to model emerging LDs that bud from membrane bilayers. A major advantage of DEVs is the ability to not only monitor membrane association, but to also examine the protein distribution and preference for droplet monolayers versus membrane bilayers.

DEVs were generated by adding the neutral lipids TAG or DAG to giant unilamellar vesicles (GUVs) of DOPC that were marked with fluorescent phospholipids **(Fig. 5A)**. As observed previously [42, 68], full-length PLIN3 was strongly recruited to the monolayer surface of triolein TAG droplets with almost no bilayer signal **(Fig. 5B, 5D)**. Addition of diolein (DO-DAG) generated small droplet buds, and full-length PLIN3 was recruited equally to the droplet and bilayer surface **(Fig. 5C, 5D)**.

Residues 1-204 of PLIN3 that contained both the PAT domain and 11-mer repeats behaved nearly identical to full-length PLIN3 in both TAG and DAG containing DEVs **(Fig. 5B, 5C and 5E)**.

Next, we tested fragments of the PAT domain and 11-mer repeats using both triolein and diolein DEVs. The 11-mer repeats preferentially bound the droplet surface of triolein DEVs with the magnitude of signal dependent on the length of the 11-mer repeats **(Fig. 5B, 5G and 5I)**. In contrast, PAT domain fragments did not bind to the droplet or bilayer surface of triolein DEVs **(Fig. 5B, 5F and 5H)**. The PAT domain was recruited to diolein DEVs, and the largest fragment (residues 1-116) bound to both the droplet and bilayer surface with similar magnitudes to fulllength PLIN3 **(Fig. 5C, 5F and 5H)**. The 11-mer repeats also bound to both the droplet and bilayer surface of diolein DEVs, but to a lesser extent **(Fig. 5C, 5G and 5I)**. These results are consistent with our previous hypothesis that the PAT domain is larger than previously expected and that this functional PAT domain binds DAG-enriched membranes, while the 11-mer repeats can also bind DAG-enriched membranes but display a preference for TAG-containing droplets over membrane bilayers.

DAG accumulation is sufficient to recruit PLIN3 to the ER in cells

DAG has previously been proposed to recruit PLIN3 to the ER in cells by blocking its hydrolysis or acylation or by the exogenous addition of DAG [69]. This is consistent with the current model for LD formation, where DAG accumulates at the site of TAG nucleation on the ER membrane [18, 19, 70], the local high concentration of neutral lipids promotes LD nucleation through Seipin [15], and cytoplasmic PLIN3 is recruited to early LDs [10, 45]. We sought to test whether DAG accumulation was sufficient for PLIN3 recruitment using an independent system and also assess what fragments of PLIN3 were necessary and sufficient for ER recruitment.

To best visualize PLIN3 recruitment to ER membranes, we generated intracellular giant ER vesicles (GERVs) by submitting cells to hypotonic medium [66, 71, 72] **(Fig. 6A)**. After exchange to hypotonic medium, cells were pretreated with DMSO or the DGAT inhibitors (DGATi), followed by oleic acid to induce TAG or DAG synthesis [72] **(Fig. 6A)**. Confocal microscopy was used to visualize cells prior and after exchange to hypotonic medium, and after oleic acid treatment. Imaging was done in the following minutes after the treatments.

As expected, the majority of subcellular localization of GFP-tagged PLIN3 was cytoplasmic in both normal and hypotonic media without addition of oleic acid **(Fig. 6B, upper panels)**, and colocalized with LDs **(Fig. 6D)**. Under conditions of DGAT inhibition, PLIN3 co-localized to the outer periphery of GERVs **(Fig. 6B, yellow arrow, 6E and 6F)**, which suggests DO-DAG accumulation is sufficient to recruit PLIN3 to ER membrane bilayers.

In line with our previous results, a construct containing both the PAT domain and 11-mer repeats showed a similar subcellular localization as full-length PLIN3 under all conditions **(Fig. 6C-6F)**. This suggests the PAT domain and 11-mer repeats are sufficient for PLIN3 recruitment to both DAG enriched membrane bilayers and TAG containing LDs, which might also contain DAG whose concentration could increase the protein binding level. Interestingly, constructs containing only the PAT domain (residues 1-116) or only the 11-mer repeats (residues 114-204), which bound to DEVs in a DAG-dependent manner, remained cytoplasmic under all conditions **(Fig. 6D, 6E, Fig. S4)**. Taken together, we concluded that PLIN3 is capable of binding both DAG enriched ER membranes and early LDs, and that the PAT domain and 11-mer repeats are both necessary and synergize to perform these functions in cells.

DISCUSSION

Here we find that PLIN3 not only binds LDs, but also membrane bilayers enriched in DAG and PA. These results are in line with other studies that revealed PLIN3 binding to DAG [69]. In our hands, DAG binding was observed with multiple in vitro systems (e.g. liposomes, DEVs) and DODAG was also sufficient for PLIN3 recruitment to the ER in cells. Cellular recruitment to membranes by DAG is consistent with a seminal study that used inhibitors to block DAG hydrolysis or acylation and exogenous DAG to promote ER recruitment of PLIN3 [69]. However, here we show that oleate addition in combination with DGAT inhibition is sufficient for the subcellular redistribution of PLIN3 to the ER, which best mimics normal the LD biogenesis pathway.

There are several mechanistic implications of PLIN3 recruitment to DAG enriched membranes. First, this implies that PLIN3 may be recruited to sites of LD formation, not only through TAG generation, but also at the very initial stages when DAG begins to accumulate. This raises the possibility that PLIN3 may play a role in early stage of LD formation by stabilizing DAG enriched regions on ER. Once PLIN3 binds to accumulated DAG, it might coat the curved surface of a growing DAG/TAG lens and regulate LD budding, in conjunction with seipin.

In this study, we attempted to clarify the function and boundaries of the PAT domain. Our HDXMS results using full-length PLIN3 clearly implicate both the PAT domain and 11-mer repeats in membrane binding. In addition, an expanded PLIN3 PAT domain is sufficient to bind DAG enriched membranes, but not LDs. In contrast, the 11-mer repeats display some affinity for DAGenriched membranes and are necessary to bind LD monolayers. Our overall conclusion is that the PAT domain and 11-mer repeats serve synergistic functions, as the individual regions are necessary for both LD and DAG recruitment in cells.

The PAT domain is predicted to adopt a triangular tertiary structure by both AlphaFold and RoseTTAfold. Our PD-ESR distance measurements are consistent with these predictions but not identical. This suggests that the PAT domain does adopt a folded domain when bound to membranes but that this domain may be dynamic and vary its structure. This conclusion is supported by our HDX-MS results that found the peptides within the PAT domain display longer protection times from H-D exchange, which is consistent with tertiary structure to provide more resistance to unfolding and longer membrane residency times.

To our knowledge, our finding that the PAT domain of PLIN3 is sufficient to bind DAG represents the first functional role for the PAT domain in any PLIN. This suggests that the highly conserved PAT domain in other PLINs may serve similar or related functions. For example, could the PAT domain be a general sensor for DAG in membrane bilayers? Or could the PAT domain of other PLINs potentially bind to other neutral lipids (e.g. CEs, TAGs, retinol esters)? Given the previously observed differing neutral lipid preference of PLINs [20] and the involvement of the PAT domain in lipid/membrane binding, this now raises the questions if this is due to the PAT domain preference, the 11-mer repeat preference, or the synergistic action of the combined PAT-11mer repeat units.

Lastly, our results are consistent with previous studies that found the PLIN3 4-helix bundle does not bind LDs, but other PLINs 4-helix bundles can bind LDs [37]. While the domain boundaries of the 4-helix bundles seem reasonable given structure of mouse PLIN3 [51], the variable membrane binding affinities we observed for the PAT domain and 11-mer repeats does raise the question if stability of 4-helix bundle, and consequently the ability to unfold and bind membranes or LDs in other PLINs may depend on the domain boundaries of specific constructs. Thus, we suggest it is reasonable to revisit the ability of the 4-helix bundles from other PLINs using constructs that can be stably purified in vitro to rule out potential artifacts from the use of unstable 4-helix bundles.

MATERIALS AND METHODS

Protein expression and purification

The genes encoding PLIN3 constructs were codon-optimized for expression in *Escherichia coli* and cloned into pTHT, which is a derivative of pET28 that contains a TEV cleavable N-terminal 6x His tag. For GFP tagged PLIN3 constructs, monomeric superfolder GFP (msfGFP) was inserted between the 6x His tag and the N-terminus of PLIN3. PLIN3 plasmids were transformed into BL21(DE3) RIPL cells and protein expression was induced with 1mM isopropyl β-D-1thiogalactopyranoside (IPTG) at 37°C for 3h. Cells was harvested by centrifugation at 3,320 x g for 20 mins and stored at -80°C until use. Cell pellets were resuspended with buffer A containing 500 mM NaCl, 20 mM Tris-HCl pH 7.5, 5% glycerol, 5 mM 2-mercaptoethanol (BME) and lysed by sonication. Cell lysates were centrifuged at 81,770 x g for 1h at 4°C and the resulting supernatant was incubated with 5 mL of Ni-NTA resin for 2h at 4°C prior to loading onto a gravity column. The Ni-NTA resin was washed with buffer B containing 500 mM NaCl, 20 mM Tris-HCl pH 7.5, 5% glycerol, 5 mM BME and 60 mM imidazole. Human PLIN3 proteins were eluted with buffer C containing 500 mM NaCl, 20 mM Tri-HCl pH 7.5, 5% glycerol, 5 mM BME and 300 mM imidazole. Eluted protein was applied to a HiLoad 26/600 Superdex 200 pg column (GE life sciences) equilibrated with 150 mM NaCl, 20 mM Tris-HCl pH 7.5, 5% glycerol, and 5 mM BME. Protein was analyzed by SDS-PAGE, concentrated using a centrifugal tube (10K MWCO, Pall Corporation), aliquoted and stored at -80°C.

Lipids

The following lipids were purchased from Avanti Polar Lipids: 1,2-dioleoyl-sn-glycero-3phosphocholine (DOPC, catalog #850375), 1,2-dioleoyl-sn-glycero-3-phosphoethanolamine (DOPE, catalog #850725), 1,2-dioleoyl-sn-glycero-3-phosphate (DOPA, catalog #840875), 1,2dioleoyl-sn-glycero-3-phospho-L-serine (DOPS, catalog #840035), 1-palmitoyl-2-oleoyl-glycero3-phosphocholine (POPC, catalog #850457), 1-palmitoyl-2-oleoyl-sn-glycero-3phosphoethanolamine (POPE, catalog #850757), 1-palmitoyl-2-oleoyl-sn-glycero-3-phosphate (POPA, catalog #840857), 1-palmitoyl-2-oleoyl-sn-glycero-3-phospho-L-serine (POPS, catalog #840034), 1,2-diphytanoyl-sn-glycero-3-phosphocholine (4ME-PC, catalog #850356), 1,2diphytanoyl-sn-glycero-3-phosphoethanolamine (4ME-PE, catalog #850402), 1,2-diphytanoyl-snglycero-3-phosphate (4ME-PA, catalog #850406), 1,2-diphytanoyl-sn-glycero-3-phospho-Lserine (4ME-PS, catalog #850408), 1-palmitoyl-2-oleoyl-sn-glycerol (DAG, catalog #800815),

Lα-phosphatidylinositol (Soy PI, catalog #84044), L-α-phosphatidylinositol-4-phosphate (Brain, Porcine (PI(4)P, catalog #840045), N-stearoyl-D-erythro-sphingosine (C18:1 ceramide, catalog #860518). 1,2,3-Trioleoyl Glycerol was purchase from Cayman Chemicals (TAG, catalog #26950).

Liposome co-sedimentation assay

To prepare liposomes, lipids were dried under a nitrogen gas stream and dissolved with buffer containing 50 mM NaCl and 50 mM HEPES pH 8.0 with a total lipid concentration of 2 mM. Liposomes were generated by repeated cycles of flash freezing in liquid nitrogen, thawing in 37°C water bath, and vortexing. For liposome co-sedimentation assays, 20 µL of 12uM purified protein was incubated with 40 µL of 2 mM liposomes for 40 min at 23°C. Protein fractions bound to liposomes were isolated by centrifugation at 100,000 x g for 70 mins at 4°C and analyzed by SDSPAGE.

Artificial lipid droplet flotation assay

Artificial lipid droplets (ALDs) were prepared by mixing phospholipids and triacylglycerols (TAGs). Di-oleoyl phospholipids were dried under a nitrogen gas stream. Dried lipids were resuspended with lipid droplet flotation assay buffer containing 50 mM NaCl and 50 mM HEPES pH 8.0 and TAGs in the molar ratio of 2:5. ALDs were formed by repeating the cycles of vortex for 10 sec and rest for 10 sec. ALDs were further vortexed before use for the assay. 100 µL of ALDs were mixed with 5 µL of human PLIN3 and 105 µL of lipid flotation assay buffer to give a final concentration of 5uM protein and 1.5 mM phospholipids. The average diameters of different ALDs were measured by dynamic light scattering (DLS). The concentration of ALDs were determined by optical density at 600 nm. The mixture of human PLIN3 and ALDs was incubated for 1h at 23°C. To generate a sucrose gradient, 140 µL of a 75% sucrose solution was added to 210 µL of the protein-ALD mixture to give a final concentration of 30% sucrose. The resulting mixture (320 µL) was transferred to an ultra-centrifuge tube. 260 µL of a 25% sucrose solution was applied on top of 30% sucrose/protein/ALDs mixture. Lastly, 60 µL of lipid flotation assay buffer was laid on the top. ALDs were floated by centrifugation at 76,000 x g for 3h at 20°C with sucrose gradient of 30% (bottom), 25% (middle), and 0 % (top). Three fractions of 100 µL from the top, 260 µL from the middle and 280 µL from the bottom were collected and analyzed by SDS-PAGE.

Hydrogen-Deuterium Exchange Mass Spectrometry (HDX-MS)

Sample preparation

HDX reactions for PLIN3 deuterium pulse were conducted in a final reaction volume of 10 µL with a final concentration 2.12 µM PLIN3. Exchange was carried out in triplicate for a single time point (3 s at 0 °C). Hydrogen deuterium exchange was initiated by the addition of 9 µl of D2O buffer solution (20 mM HEPES pH 7, 100 mM NaCl) to 1 µl of protein, to give a final concentration of 84.9% D2O. Exchange was terminated by the addition of acidic quench buffer at a final concentration 0.6 M guanidine-HCl and 0.9% formic acid. Samples were immediately frozen in liquid nitrogen at -80 °C. Fully deuterated samples were generated by first denaturing the protein in 6M guanidine for 1 hour at 20°C. Following denaturing, 9 µL of D2O buffer was added to the denatured protein and allowed to incubate for 10 minutes at 20°C before quenching with 0.6 M guanidine-HCl and 0.9% formic acid. Samples were immediately frozen in liquid nitrogen at -80 °C, and all timepoints were created and run in triplicate.

HDX reactions comparing PLIN3 in the presence of PA liposomes (60% 4ME-PC, 20% 4ME-PE, 20% 4ME-PA) were conducted in a final reaction volume of 10 µL with a final protein concentration of 3µM and final liposome concentration of 1mM. Protein and liposomes were preincubated together for 2 minutes at room temperature before the addition of 7ul D2O buffer solution (50 mM HEPES pH 8, 50 mM NaCl) for a final concentration of 72% D2O. Exchange was carried out for 3s, 30s, 300s and 3000s, and exchange was terminated by the addition of acidic quench buffer at a final concentration 0.6 M guanidine-HCl and 0.9% formic acid. Samples were immediately frozen in liquid nitrogen at -80 °C, and all timepoints were created and run in triplicate.

HDX reactions comparing PLIN3 in the presence of two different liposomes (60% DOPC, 20% DOPE, 20% DAG liposomes and 80% 4ME-PC, 20% 4ME-PE liposomes) were conducted in a final reaction volume of 10 µL with a final protein concentration of 3µM and final liposome concentration of 500uM. Protein and liposomes were preincubated together for 2 minutes at room temperature before the addition of 8ul D2O buffer solution (20 mM HEPES pH 7, 100 mM NaCl) for a final concentration of 72% D2O. Exchange was carried out for 3s, 30s, 300s and 3000s, and exchange was terminated by the addition of acidic quench buffer at a final concentration 0.6 M guanidine-HCl and 0.9% formic acid. Samples were immediately frozen in liquid nitrogen at -80 °C, and all timepoints were created and run in triplicate.

Protein digestion and MS/MS data collection

Protein samples were rapidly thawed and injected onto an integrated fluidics system containing a HDx-3 PAL liquid handling robot and climate-controlled (2°C) chromatography system (LEAP Technologies), a Dionex Ultimate 3000 UHPLC system, as well as an Impact HD QTOF Mass spectrometer (Bruker). The protein was run over either one (at 10°C) or two (at 10°C and 2°C) immobilized pepsin columns (Trajan; ProDx protease column, 2.1 mm x 30 mm PDX.PP01-F32) at 200 µL/min for 3 minutes. The resulting peptides were collected and desalted on a C18 trap column (Acquity UPLC BEH C18 1.7mm column (2.1 x 5 mm); Waters 186003975). The trap was subsequently eluted in line with an ACQUITY 1.7 µm particle, 100 × 1 mm2 C18 UPLC column (Waters), using a gradient of 3-35% B (Buffer A 0.1% formic acid; Buffer B 100% acetonitrile) over 11 minutes immediately followed by a gradient of 35-80% over 5 minutes. Mass spectrometry experiments acquired over a mass range from 150 to 2200 m/z using an electrospray ionization source operated at a temperature of 200C and a spray voltage of 4.5 kV.

Peptide identification

Peptides were identified from the non-deuterated samples of PLIN3 using data-dependent acquisition following tandem MS/MS experiments (0.5 s precursor scan from 150-2000 m/z; twelve 0.25 s fragment scans from 150-2000 m/z). MS/MS datasets were analyzed using PEAKS7 (PEAKS), and peptide identification was carried out by using a false discovery based approach, with a threshold set to 1% using a database of known contaminants found in Sf9 and E. coli cells [73]. The search parameters were set with a precursor tolerance of 20 ppm, fragment mass error 0.02 Da, charge states from 1-8, leading to a selection criterion of peptides that had -10logP scores of 22.8 for the pulse experiment and 20.9 for the liposome experiment.

Mass Analysis of Peptide Centroids and Measurement of Deuterium Incorporation

HD-Examiner Software (Sierra Analytics) was used to automatically calculate the level of deuterium incorporation into each peptide. All peptides were manually inspected for correct charge state, correct retention time, appropriate selection of isotopic distribution, etc. Deuteration levels were calculated using the centroid of the experimental isotope clusters. Results are presented as relative levels of deuterium incorporation, with the only correction being applied correcting for the deuterium oxide percentage of the buffer utilized in the exchange (84.9% and 72%). Differences in exchange in a peptide were considered significant if they met all three of the

following criteria: : ≥5% change in exchange and ≥0.4 Da difference in exchange. The raw HDX data are shown in two different formats. Samples were only compared within a single experiment and were never compared to experiments completed at a different time with a different final D2O level. The data analysis statistics for all HDX-MS experiments are in Supplemental Table 1 according to the guidelines of [74]. The mass spectrometry proteomics data have been deposited to the ProteomeXchange Consortium via the PRIDE partner repository with the dataset identifier PXD025717 [75].

Site-directed spin-labeling

Recombinant PLIN3 cysteine-substituted proteins were purified using Ni-NTA resin in a buffer 500mM NaCl, 20mM Tris pH7.5, 5% glycerol and eluted in a buffer of 500mM NaCl, 20mM Tris pH7.5, 5% Glycerol, 300mM imidazole. Elution was spin-labeled with 1 µg/mL (S-(1-oxyl-2,2,5,5tetramethyl-2,5-dihydro-1H-pyrrol-3-yl) methyl methanesulfonothioate), MTSL, (Santa Cruz Biotech) dissolved in acetonitrile at 4°C overnight. The spin-labeled proteins were further purified by HiLoad 26/600 Superdex 200 pg column (GE life sciences) in a buffer of 150 mM NaCl, 20 mM Tris pH 7.5 to remove unreacted spin labels.

Sample preparations for DEER spectroscopy

Protein samples in solutions were prepared at ca. 40-60 µM concentrations in 20 mM Tris at pH 7.5, 150 mM NaCl, and 40 vol% glycerol. Liposome samples containing 10 µM protein and 3.33 mM lipid were prepared by mixing 30 µM protein stocks with 5 mM liposome solutions using 1 to 2 aliquots followed by 30 min incubation at RT. The liposomes were freshly prepared by rehydration of lyophilized 80/20 mol% 4ME-PC/PE followed by seven freeze-thaw cycles. Freshly-prepared 20 µL amounts of spin-labeled samples were loaded into 1.8 mm inner diameter Pyrex sample tubes (Wilmad-LabGlass), frozen by plunging in liquid nitrogen, and stored in liquid nitrogen for PDS measurements.

DEER data collection and analysis

PDS DEER measurements were performed at 60 K with a home-built Ku band pulse ESR spectrometer operating around 17.3 GHz [59, 76]. A four-pulse DEER sequence [77] was employed using for spin-echo detection p/2- and p-pulses with respective widths of 16 and 32 ns, the p-pulse for pumping was 16 ns. The detection frequency matched the peak at the low-field

spectral edge, while pumping was performed at a lower by 70 MHz frequency, corresponding to the central maximum. A 32-step phase cycle [78] was applied to suppress unwanted contributions to the signal. Nuclear electron spin-echo envelope modulation (ESEEM) caused by surrounding protons was suppressed using the data from four measurements. In this method the initial pulse separations and the start of detection were advanced by 9.5 ns in subsequent measurements, i.e. by the quarter period of the 26.2 MHz nuclear Zeeman frequency for protons at 0.615 T corresponding to the working frequency. The four signal traces were summed to achieve deep suppression of nuclear ESEEM, [79].

The solution samples had phase memory times, T_m's, of about 2.5 μs, so the data could be recorded up to 3 μs evolution time (t_m). Such evolution times did not provide sufficient decay of the dipolar coherence to the background level, providing however clear indication of unstructured nature of the protein in solution. Any residual secondary structure could be probed by using multiple labeling sites, however other techniques did not encourage this undertaking. For solutions the DEER data were acquired in less than 12 hr. Faster phase relaxation times (~1 μs) and low spin concentrations in liposome samples required signal averaging for ~24 h to facilitate good reconstruction by Tikhonov regularization. [80, 81]

For liposomes, time domain DEER data, $V(t)$, were recorded and preprocessed using standard approaches [57, 60, 77, 82] before their reconstruction into distance distributions, $P(r)$'s. The first step is to remove signal decay caused by intermolecular dipole-dipole couplings, followed by subtracting the residual background from the spins whose partner was not flipped by the pump or missing. This was done, as usual, by fitting the latter points (about a half of the record) of $\ln[V(t)]$ to a low-order polynomial, usually a straight line for solutions (and often for liposomes), extrapolating it to zero time, and subtracting out from $\ln[V(t)]$; so that the antilog yields $u(t) = d(t) + 1$. Here $d(t)$ is the dipolar evolution representing part. Once $u(t)$ is normalized as $u(t)/u(0)$, it serves as a typical form of DEER data presentation, while $v(t)=(u(t)-1)/u(0)$, gives backgroundfree "dipolar" data to be converted to a distance distribution between spins in pairs. We used Lcurve Tikhonov regularization [80] for distance reconstruction. The Tikhonov regularization utility allowed selection of either the signal or its derivatives in the Tikhonov functional and selection of the regularization parameter. The latter increases $P(r)$ smoothness at the expense of introducing some broadening.

Dipolar signal amplitude ("modulation depth") is given by $v(0)$. This would be accurate to the extent the background or $V(\infty)$, the asymptotic value of $V(t)$, is known. This depth, tabulated by calculations for typical pulse sequence setup and verified in numerous experiments, is a measure of a fraction of spins in pairs or oligomers [63, 83, 84]. It is thus useful in estimate of spin-labeling efficiency and protein concentration.

Cell culture

Cos7 cells were maintained in Dulbecco's modified Eagle's medium (DMEM) supplemented with 10% heat inactivated fetal bovine serum (Life Technologies), 4.5 gL^{-1} D-glucose, 0.1 gL^{-1} sodium pyruvate (Life Technologies) and 1% penicillin-streptomycin (Life Technologies). The cells were cultured at 37°C under a 5% CO2 atmosphere.

Transfection

When indicated, Cos7 cells (60–70% confluence) plated into a 35 mm cell-culture Mattek dishes (with a glass coverslip at the bottom), (MatTek Corp. Ashland, MA). were transfected with 3µg of plasmid DNA/ml using Polyethylenimine HCl MAX (Polysciences) following the manufacturer's instructions. For co-expressions, RFP-KDEL or GFP-Plin3 constructs in equal concentrations (1.5–2 µg for each one) were transfected to cells 24hr prior observation.

Giant unilamellar vesicles, GUVs

GUVs were prepared by electroformation following the protocol described in [85]. Phospholipids, dioleoyl phosphatidylcholine (PC) (70%) and dioleoyl phosphatidylethanolamine (PE) (29%), Rhodamine-DOPE 1% (w/w)), were purchased from Avanti Polar Lipids. The lipid mixture, in chloroform at 0.5 mM, was dried on an indium tin oxide (ITO)-coated glass plate. The lipid film was desiccated for 1 h. The chamber was sealed with another ITO- coated glass plate. The lipids were then rehydrated with a sucrose solution (275 mOsm). Electroformation was done using 100 Hz AC voltage at 1.0 to 1.4 Vpp and maintained for at least 1 h.

Droplet-embedded vesicles (DEVs) preparation

Artificial LDs (aLDs) were prepared in HKM buffer: 50 mM Hepes, 120 mM Kacetate, and 1 mM MgCl2 (in Milli-Q water) at pH 7.4 and 275±15 mOsm. To do so, 5µL of the lipid oil solution (triolein or diacylglycerol purchased from Sigma) was added to 45 mL of HKM buffer and the mixture was sonicated as described in [86]. The resulting emulsion was then mixed with GUVs for five minutes

under rotator to generate DEVs [86]. DEVs were then placed on a glass coverslip pretreated with 10%(w/w) BSA and washed three times with buffer.

Protein binding to DEVs

For the protein binding experiments, 50μL HKM were deposited on the BSA-treated glass, 30μL of the DEV solution added and 1.5μL purified Plin3 or Plin3 fragments added (in the case of 107204 and 1-106 fragments, 3μL were added). The final protein concentration in the solution was between 1μM to 4μM depending on the protein. For quantifications, 10-15 DEVs were considered and the signal on the droplet and bilayer was determined by Fiji, via drawing 5-10 points-thick line profiles.

Neutral lipid synthesis induction

Wherever relevant, cells were exposed for 1 h to 350 μM oleic acid (OA) coupled to bovine serum albumin (BSA) (1% vol/vol) to induce neutral lipids' synthesis. LipidTox DeepRed (Thermo Fischer), was used to visualize lipid droplets or membranes enriched in neutral lipids.

Giant Intra-Cellular ER vesicle experiments

For GERV experiments, Cos7 cells were first transfected for 24 h with the indicated eGFP plasmids and RFP-KDEL. The culture media of the cells was next replaced by a hypotonic culture media (DMEM:H2O, 1:20). The cells were then incubated at 37°C, 5% CO2 for 5 minutes, to induce GERVs, and then they were visualized. Neutral lipids' synthesis was triggered by the addition of OA and Z-stacks imaging of different entire cells was performed before and 15 min after OA administration, as described in [72]. For the DGAT1 (Sigma, PF-04620110) and DGAT2 (Sigma, PF-06424439) inhibitors used in Cos7, the dilution applied was 1/1000 for a final concentration of 3ug/mL. In the GERV protocol, the inhibitors were added to the cell medium before cell transfection or during the hypotonic solution addition. The signal of Plin3 or fragments thereof was quantified for tens of GERVs by depicting the mean signal on the GERVs to which was subtracted the bulk cytosolic signal; this resulted signal was normalized to the cytosolic signal.

REFERENCES

1. Thiam, A.R., R.V. Farese, Jr., and T.C. Walther, *The biophysics and cell biology of lipid droplets.* Nat Rev Mol Cell Biol, 2013. **14**(12): p. 775-86.
2. Rubin, C.S., et al., *Development of hormone receptors and hormonal responsiveness in vitro. Insulin receptors and insulin sensitivity in the preadipocyte and adipocyte forms of 3T3-L1 cells.* J Biol Chem, 1978. **253**(20): p. 7570-8.
3. Gibbons, G.F., K. Islam, and R.J. Pease, *Mobilisation of triacylglycerol stores.* Biochim Biophys Acta, 2000. **1483**(1): p. 37-57.
4. Olzmann, J.A. and P. Carvalho, *Dynamics and functions of lipid droplets.* Nat Rev Mol Cell Biol, 2019. **20**(3): p. 137-155.
5. Valm, A.M., et al., *Applying systems-level spectral imaging and analysis to reveal the organelle interactome.* Nature, 2017. **546**(7656): p. 162-167.
6. Miyanari, Y., et al., *The lipid droplet is an important organelle for hepatitis C virus production.* Nat Cell Biol, 2007. **9**(9): p. 1089-97.
7. Ben M'barek, K., et al., *ER Membrane Phospholipids and Surface Tension Control Cellular Lipid Droplet Formation.* Dev Cell, 2017. **41**(6): p. 591-604 e7.
8. Choudhary, V., et al., *A conserved family of proteins facilitates nascent lipid droplet budding from the ER.* J Cell Biol, 2015. **211**(2): p. 261-71.
9. Thiam, A.R. and L. Foret, *The physics of lipid droplet nucleation, growth and budding.* Biochim Biophys Acta, 2016. **1861**(8 Pt A): p. 715-22.
10. Chung, J., et al., *LDAF1 and Seipin Form a Lipid Droplet Assembly Complex.* Dev Cell, 2019. **51**(5): p. 551-563 e7.
11. Gao, M., et al., *The biogenesis of lipid droplets: Lipids take center stage.* Prog Lipid Res, 2019. **75**: p. 100989.
12. Chorlay, A., et al., *Membrane Asymmetry Imposes Directionality on Lipid Droplet Emergence from the ER.* Dev Cell, 2019. **50**(1): p. 25-42 e7.
13. Wang, H., et al., *Seipin is required for converting nascent to mature lipid droplets.* Elife, 2016. **5**.
14. Salo, V.T., et al., *Seipin regulates ER-lipid droplet contacts and cargo delivery.* EMBO J, 2016. **35**(24): p. 2699-2716.
15. Zoni, V., et al., *Pre-existing bilayer stresses modulate triglyceride accumulation in the ER versus lipid droplets.* Elife, 2021. **10**.
16. Yan, R., et al., *Human SEIPIN Binds Anionic Phospholipids.* Dev Cell, 2018. **47**(2): p. 248256 e4.
17. Guyard, V., et al., *ORP5 and ORP8 orchestrate lipid droplet biogenesis and maintenance at ER-mitochondria contact sites.* J Cell Biol, 2022. **221**(9).
18. Choudhary, V., et al., *Seipin and Nem1 establish discrete ER subdomains to initiate yeast lipid droplet biogenesis.* J Cell Biol, 2020. **219**(7).
19. Choudhary, V., et al., *Architecture of Lipid Droplets in Endoplasmic Reticulum Is Determined by Phospholipid Intrinsic Curvature.* Curr Biol, 2018. **28**(6): p. 915-926 e9.

20. Hsieh, K., et al., *Perilipin family members preferentially sequester to either triacylglycerol-specific or cholesteryl-ester-specific intracellular lipid storage droplets.* J Cell Sci, 2012. **125**(Pt 17): p. 4067-76.
21. Wolins, N.E., D.L. Brasaemle, and P.E. Bickel, *A proposed model of fat packaging by exchangeable lipid droplet proteins.* FEBS Lett, 2006. **580**(23): p. 5484-91.
22. Brasaemle, D.L., *Thematic review series: adipocyte biology. The perilipin family of structural lipid droplet proteins: stabilization of lipid droplets and control of lipolysis.* J Lipid Res, 2007. **48**(12): p. 2547-59.
23. Greenberg, A.S., et al., *Perilipin, a major hormonally regulated adipocyte-specific phosphoprotein associated with the periphery of lipid storage droplets.* J Biol Chem, 1991. **266**(17): p. 11341-6.
24. Jiang, H.P. and G. Serrero, *Isolation and characterization of a full-length cDNA coding for an adipose differentiation-related protein.* Proc Natl Acad Sci U S A, 1992. **89**(17): p. 7856-60.
25. Diaz, E. and S.R. Pfeffer, *TIP47: a cargo selection device for mannose 6-phosphate receptor trafficking.* Cell, 1998. **93**(3): p. 433-43.
26. Wolins, N.E., et al., *Adipocyte protein S3-12 coats nascent lipid droplets.* J Biol Chem, 2003. **278**(39): p. 37713-21.
27. Sztalryd, C. and D.L. Brasaemle, *The perilipin family of lipid droplet proteins: Gatekeepers of intracellular lipolysis.* Biochim Biophys Acta Mol Cell Biol Lipids, 2017. **1862**(10 Pt B): p. 1221-1232.
28. Wilson, M.H., S.C. Ekker, and S.A. Farber, *Imaging cytoplasmic lipid droplets in vivo with fluorescent perilipin 2 and perilipin 3 knock-in zebrafish.* Elife, 2021. **10**.
29. Nguyen, K.T., et al., *N-terminal acetylation and the N-end rule pathway control degradation of the lipid droplet protein PLIN2.* J Biol Chem, 2019. **294**(1): p. 379-388.
30. Takahashi, Y., et al., *Perilipin2 plays a positive role in adipocytes during lipolysis by escaping proteasomal degradation.* Sci Rep, 2016. **6**: p. 20975.
31. Masuda, Y., et al., *ADRP/adipophilin is degraded through the proteasome-dependent pathway during regression of lipid-storing cells.* J Lipid Res, 2006. **47**(1): p. 87-98.
32. Xu, G., C. Sztalryd, and C. Londos, *Degradation of perilipin is mediated through ubiquitination-proteasome pathway.* Biochim Biophys Acta, 2006. **1761**(1): p. 83-90.
33. Lee, B., et al., *Differential association of adipophilin and TIP47 proteins with cytoplasmic lipid droplets in mouse enterocytes during dietary fat absorption.* Biochim Biophys Acta, 2009. **1791**(12): p. 1173-80.
34. Rowe, E.R., et al., *Conserved Amphipathic Helices Mediate Lipid Droplet Targeting of Perilipins 1-3.* J Biol Chem, 2016. **291**(13): p. 6664-78.
35. Copic, A., et al., *A giant amphipathic helix from a perilipin that is adapted for coating lipid droplets.* Nat Commun, 2018. **9**(1): p. 1332.
36. Mirheydari, M., et al., *Insertion of perilipin 3 into a glycero(phospho)lipid monolayer depends on lipid headgroup and acyl chain species.* J Lipid Res, 2016. **57**(8): p. 1465-76.
37. Ajjaji, D., et al., *Dual binding motifs underpin the hierarchical association of perilipins1-3 with lipid droplets.* Mol Biol Cell, 2019. **30**(5): p. 703-716.

38. Bigay, J. and B. Antonny, *Curvature, lipid packing, and electrostatics of membrane organelles: defining cellular territories in determining specificity.* Dev Cell, 2012. **23**(5): p. 886-95.
39. Fujimoto, Y., et al., *Long-chain fatty acids induce lipid droplet formation in a cultured human hepatocyte in a manner dependent of Acyl-CoA synthetase.* Biol Pharm Bull, 2006. **29**(11): p. 2174-80.
40. Harayama, T. and H. Riezman, *Understanding the diversity of membrane lipid composition.* Nat Rev Mol Cell Biol, 2018. **19**(5): p. 281-296.
41. Radhakrishnan, A., et al., *Switch-like control of SREBP-2 transport triggered by small changes in ER cholesterol: a delicate balance.* Cell Metab, 2008. **8**(6): p. 512-21.
42. Caillon, L., et al., *Triacylglycerols sequester monotopic membrane proteins to lipid droplets.* Nat Commun, 2020. **11**(1): p. 3944.
43. Garten, M., et al., *Methyl-branched lipids promote the membrane adsorption of alphasynuclein by enhancing shallow lipid-packing defects.* Phys Chem Chem Phys, 2015. **17**(24): p. 15589-97.
44. Bulankina, A.V., et al., *TIP47 functions in the biogenesis of lipid droplets.* J Cell Biol, 2009. **185**(4): p. 641-55.
45. Wolins, N.E., et al., *S3-12, Adipophilin, and TIP47 package lipid in adipocytes.* J Biol Chem, 2005. **280**(19): p. 19146-55.
46. Chorlay, A., L. Foret, and A.R. Thiam, *Origin of gradients in lipid density and surface tension between connected lipid droplet and bilayer.* Biophys J, 2021. **120**(24): p. 54915503.
47. Englander, S.W. and N.R. Kallenbach, *Hydrogen exchange and structural dynamics of proteins and nucleic acids.* Q Rev Biophys, 1983. **16**(4): p. 521-655.
48. Skinner, J.J., et al., *Protein hydrogen exchange: testing current models.* Protein Sci, 2012. **21**(7): p. 987-95.
49. Balasubramaniam, D. and E.A. Komives, *Hydrogen-exchange mass spectrometry for the study of intrinsic disorder in proteins.* Biochim Biophys Acta, 2013. **1834**(6): p. 1202-9.
50. Vadas, O., et al., *Using Hydrogen-Deuterium Exchange Mass Spectrometry to Examine Protein-Membrane Interactions.* Methods Enzymol, 2017. **583**: p. 143-172.
51. Hickenbottom, S.J., et al., *Structure of a lipid droplet protein; the PAT family member TIP47.* Structure, 2004. **12**(7): p. 1199-207.
52. Weis, D.D., et al., *Identification and characterization of EX1 kinetics in H/D exchange mass spectrometry by peak width analysis.* J Am Soc Mass Spectrom, 2006. **17**(11): p. 1498-1509.
53. Jumper, J., et al., *Highly accurate protein structure prediction with AlphaFold.* Nature, 2021. **596**(7873): p. 583-589.
54. Baek, M., et al., *Accurate prediction of protein structures and interactions using a threetrack neural network.* Science, 2021. **373**(6557): p. 871-876.
55. Milov, A., K. Salikhov, and M. Shirov, *Application of ELDOR in electron-spin echo for paramagnetic center space distribution in solids.* Fizika Tverdogo Tela, 1981. **23**(4): p. 975-982.

56. Pannier, M., et al., *Characterization of Ionic Clusters in Different Ionically Functionalized Diblock Copolymers by CW EPR and Four-Pulse Double Electron−Electron Resonance.* Macromolecules, 2001. **34**(16): p. 5555-5560.
57. Borbat, P.P. and J.H. Freed, *Pulse Dipolar Electron Spin Resonance: Distance Measurements*, in *Structural Information from Spin-Labels and Intrinsic Paramagnetic Centres in the Biosciences*, C.R. Timmel and J.R. Harmer, Editors. 2014. p. 1-82.
58. Borbat, P.P. and J.H. Freed, *Dipolar Spectroscopy - Single-resonance Methods.* Emagres, 2017. **6**(4): p. 465-493.
59. Borbat, P.P., E.R. Georgieva, and J.H. Freed, *Improved Sensitivity for Long-Distance Measurements in Biomolecules: Five-Pulse Double Electron-Electron Resonance.* Journal of Physical Chemistry Letters, 2013. **4**(1): p. 170-175.
60. Jeschke, G., *DEER Distance Measurements on Proteins*, in *Annual Review of Physical Chemistry, Vol 63*, M.A. Johnson and T.J. Martinez, Editors. 2012. p. 419-446.
61. Bahrenberg, T., et al., *rDEER: A Modified DEER Sequence for Distance Measurements Using Shaped Pulses.* Magnetochemistry, 2019. **5**(1).
62. Tong, J.S., et al., *A scissors mechanism for stimulation of SNARE-mediated lipid mixing by cholesterol.* Proceedings of the National Academy of Sciences of the United States of America, 2009. **106**(13): p. 5141-5146.
63. Georgieva, E.R., et al., *Mechanism of influenza A M2 transmembrane domain assembly in lipid membranes.* Sci Rep, 2015. **5**: p. 11757.
64. Borbat, P., et al., *Inter-helix distances in lysophospholipid micelle-bound alpha-synuclein from pulsed ESR measurements.* Journal of the American Chemical Society, 2006. **128**(31): p. 10004-10005.
65. Jeschke, G., et al., *Interresidual distance determination by four-pulse double electronelectron resonance in an integral membrane protein: the Na+/proline transporter PutP of Escherichia coli.* Biophysical Journal, 2004. **86**(4): p. 2551-2557.
66. Santinho, A., et al., *Membrane Curvature Catalyzes Lipid Droplet Assembly.* Curr Biol, 2020. **30**(13): p. 2481-2494 e6.
67. Chorlay, A. and A.R. Thiam, *Neutral lipids regulate amphipathic helix affinity for model lipid droplets.* J Cell Biol, 2020. **219**(4).
68. Ma, X., et al., *Validating an artificial organelle: Studies of lipid droplet-specific proteins on adiposome platform.* iScience, 2021. **24**(8): p. 102834.
69. Skinner, J.R., et al., *Diacylglycerol enrichment of endoplasmic reticulum or lipid droplets recruits perilipin 3/TIP47 during lipid storage and mobilization.* J Biol Chem, 2009. **284**(45): p. 30941-8.
70. Joshi, A.S., et al., *Lipid droplet and peroxisome biogenesis occur at the same ER subdomains.* Nat Commun, 2018. **9**(1): p. 2940.
71. King, C., et al., *ER membranes exhibit phase behavior at sites of organelle contact.* Proc Natl Acad Sci U S A, 2020. **117**(13): p. 7225-7235.
72. Ajjaji, D., et al., *Hepatitis C virus core protein uses triacylglycerols to fold onto the endoplasmic reticulum membrane.* Traffic, 2022. **23**(1): p. 63-80.

73. Dobbs, J.M., M.L. Jenkins, and J.E. Burke, *Escherichia coli and Sf9 Contaminant Databases to Increase Efficiency of Tandem Mass Spectrometry Peptide Identification in Structural Mass Spectrometry Experiments.* J Am Soc Mass Spectrom, 2020. **31**(10): p. 2202-2209.
74. Masson, G.R., et al., *Recommendations for performing, interpreting and reporting hydrogen deuterium exchange mass spectrometry (HDX-MS) experiments.* Nat Methods, 2019. **16**(7): p. 595-602.
75. Perez-Riverol, Y., et al., *The PRIDE database and related tools and resources in 2019: improving support for quantification data.* Nucleic Acids Res, 2019. **47**(D1): p. D442D450.
76. Borbat, P.P., R.H. Crepeau, and J.H. Freed, *Multifrequency two-dimensional Fourier transform ESR: an X/Ku-band spectrometer.* J Magn Reson, 1997. **127**(2): p. 155-67.
77. Jeschke, G. and Y. Polyhach, *Distance measurements on spin-labelled biomacromolecules by pulsed electron paramagnetic resonance.* Physical Chemistry Chemical Physics, 2007. **9**(16): p. 1895-1910.
78. Gamliel, D. and J.H. Freed, *THEORY OF 2-DIMENSIONAL ESR WITH NUCLEAR MODULATION.* Journal of Magnetic Resonance, 1990. **89**(1): p. 60-93.
79. Tang, S.G., et al., *Structural basis for activation, assembly and membrane binding of ESCRT-III Snf7 filaments.* Elife, 2015. **4**.
80. Chiang, Y.W., P.P. Borbat, and J.H. Freed, *The determination of pair distance distributions by pulsed ESR using Tikhonov regularization.* Journal of Magnetic Resonance, 2005. **172**(2): p. 279-295.
81. Chiang, Y.W., P.P. Borbat, and J.H. Freed, *Maximum entropy: a complement to Tikhonov regularization for determination of pair distance distributions by pulsed ESR.* Journal of magnetic resonance (San Diego, Calif.: 1997), 2005a. **177**(2): p. 184-196.
82. Borbat, P.P. and J.H. Freed, *Measuring distances by pulsed dipolar ESR spectroscopy: spin-labeled histidine kinases.* Methods Enzymol, 2007. **423**: p. 52-116.
83. Bode, B.E., et al., *Counting the monomers in nanometer-sized oligomers by pulsed electron - Electron double resonance.* Journal of the American Chemical Society, 2007. **129**(21): p. 6736-6745.
84. Milov, A.D., A.B. Ponomarev, and Y.D. Tsvetkov, *Modulation beats of signal of double electron-electron resonance in spin echo for biradical systems* Journal of Structural Chemistry, 1984. **25**(5): p. 710-713.
85. Thiam, A.R., et al., *COPI buds 60-nm lipid droplets from reconstituted waterphospholipid-triacylglyceride interfaces, suggesting a tension clamp function.* Proc Natl Acad Sci U S A, 2013. **110**(33): p. 13244-9.
86. Chorlay, A., A. Santinho, and A.R. Thiam, *Making Droplet-Embedded Vesicles to Model Cellular Lipid Droplets.* STAR Protoc, 2020. **1**(3): p. 100116.

Acknowledgements

This work was supported by in part by the NIGMS (R35GM128666, MVA), the Sloan Research Foundation (MVA), the Natural Science and Engineering Research Council of Canada (Discovery Grant 2020-04241, JEB) with salary support from the Michael Smith Foundation for Health Research (Scholar award 17868, JEB), and ANR (18-CE11-0012-01-MOBIL, CE110032-02-LIPRODYN and 21-CE13-0014-LIPDROPER, ART). ESR study, conducted at ACERT, was supported by NIH/NIGMS grants 1R24GM146107 and P41GM103521.

Author contributions

YMC generated constructs for E. coli and mammalian cell expression, purified all proteins, conducted liposome sedimentation and artificial lipid droplet binding assays, prepared figures, and wrote the initial draft. DA conducted all DEV and cell culture experiments. KDF, MLJ, and BEM setup, analyzed, and/or prepared figures and text from the HDX-MS data. PPB designed, acquired, and analyzed all PDS-ESR data. JEB, ART, JHF and MVA supervised the work and provided funding support.

Competing Interest Statement

JEB reports personal fees from Scorpion Therapeutics and Olema Oncology; and research grants from Novartis.

Figures and Figure Legends

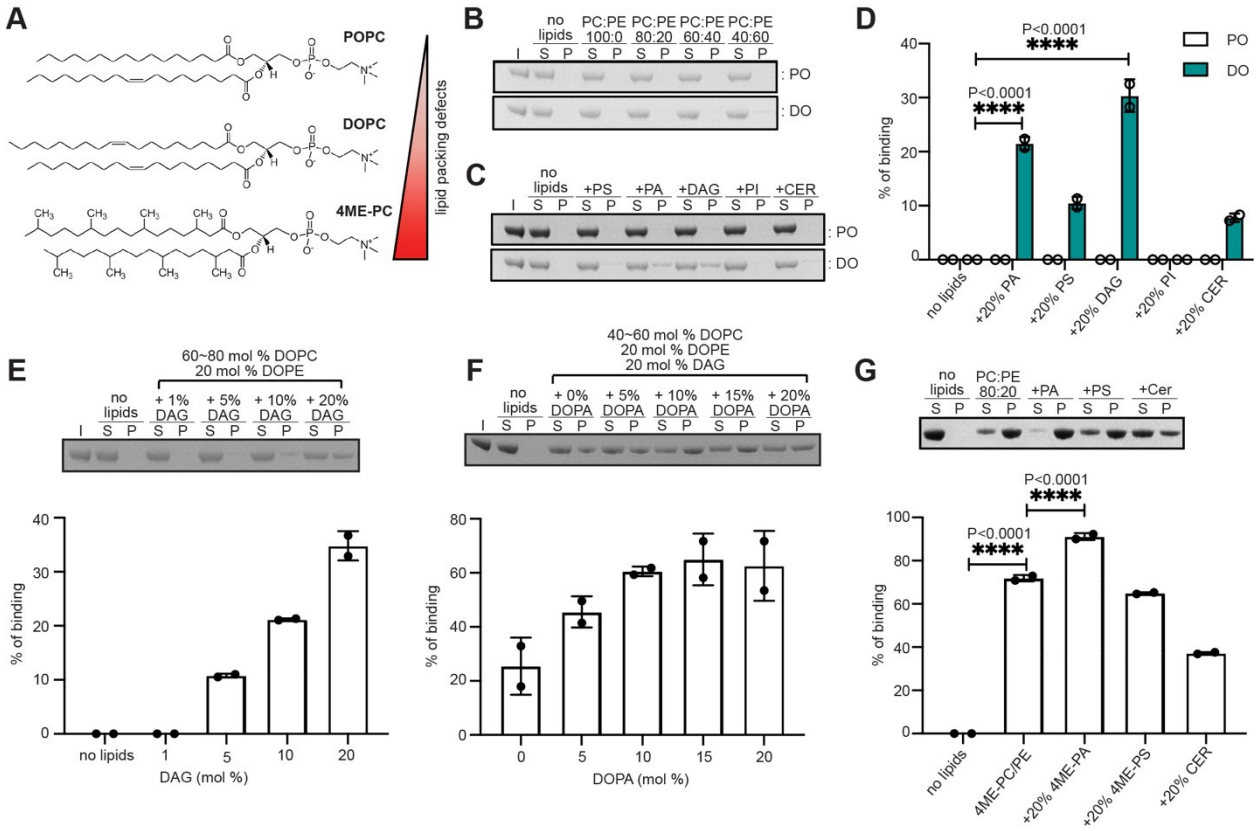

Figure 1. Triglyceride precursors DAG and PA recruit PLIN3 to membrane bilayers

A) Structures of representative phospholipids used in this study.

B) SDS-PAGE analysis of human PLIN3 liposome sedimentation assay on the either palmitoyloleoyl (PO)-liposomes or di-oleoyl (DO)-liposomes in different ratio of PC to PE. Lane S (supernatant) and P (pellet) represent unbound and bound human PLIN3 to liposomes.

C) SDS-PAGE analysis of human PLIN3 recruitment to liposomes enriched with 20 mol% of the additional lipids PS, PA, DAG, PI and ceramide.

D) Quantification of PLIN3 recruitment to liposomes in different lipid compositions (n=2). Statistical analysis was performed using two-way ANOVA (****, p<0.0001).

E) SDS-PAGE analysis of human PLIN3 recruitment to DO-liposomes using different amounts of DAG. DOPE concentration was held constant at 20 mol% and DOPC was adjusted between 60 and 80 mol% to maintain total phospholipid concentration. Bar graph shows addition of DAG increases PLIN3 binding.

F) SDS-PAGE analysis of human PLIN3 recruitment to DO-liposomes enriched with different amount of DOPA. The amounts of DOPE and DAG were kept constant at 20 mol%. DOPC concentration was adjusted between 40 and 60 mol% to maintain total phospholipid concentration. Bar graph shows addition of DOPA further increases PLIN3 binding.

G) SDS-PAGE analysis of human PLIN3 recruitment to 4ME liposomes enriched with 20 mol% of the additional lipids 4ME-PA, 4ME-PS, ceramide. 4ME-PC and 4ME-PE concentrations ranged between 60 ~80 mol% and 20 mol%, respectively. Statistical analysis for quantification of liposome binding was performed using ordinary one-way ANOVA with Tukey's multiple comparison test (n=2, ****,p<0.0001)

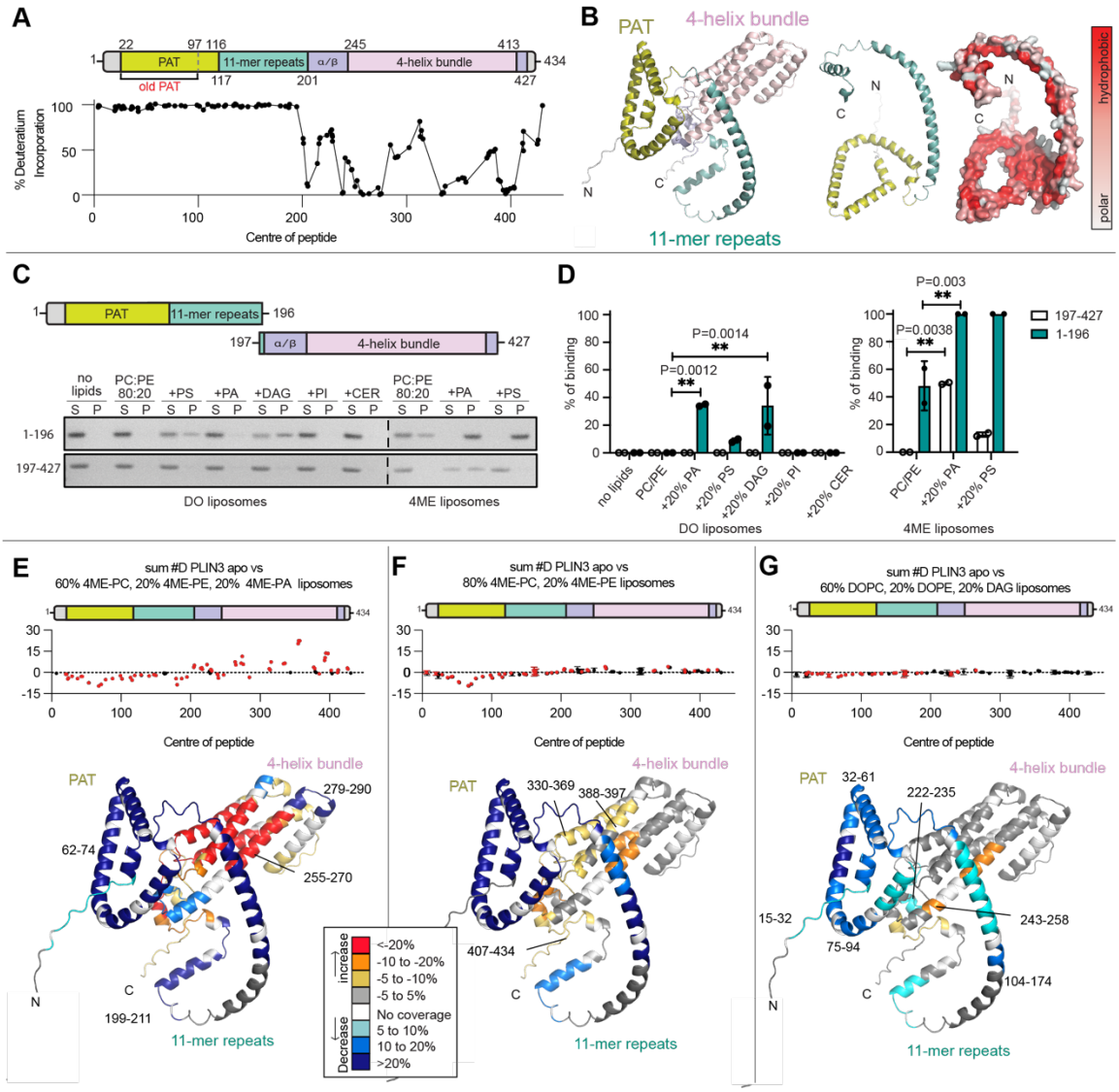

Figure 2. HDX-MS analysis of PLIN3 membrane binding

A) Absolute percentage of deuterium incorporation after 3 sec deuterium exposure of PLIN3 at 1°C in the absence of liposomes. Each point represents a single peptide, with them being graphed on the x-axis according to their central residue. A domain architecture of human PLIN3 was drawn to match the scale of x-axis of HDX-MS. N-terminal PAT domain (mustard) and 11mer repeats (cyan) have no detectable secondary structure in the absence of liposomes.
B) A predicted 3D structure of human PLIN3 by alphaFold (Left). The surface of PAT domain and 11-mer repeats were shown according to the hydrophobicity (Right).
C) SDS-PAGE and **D)** quantitative analysis of PAT/11-mer repeats and 4-helix bundle liposome binding. DO and 4ME-liposomes were prepared in the same way as Figure 1C and 1D. Statistical analysis for quantification of liposome binding was performed using two-way ANOVA with Tukey's multiple comparison test (n=2).
E-G) Quantitative analysis of deuterium exchange differences of human PLIN3 in the presence of liposomes. The sum of the difference in the # of incorporated deuterons is shown for the

absence and the presence of liposomes over all timepoints. The N-terminus composed of PAT/11-mer repeats was significantly protected from deuterium exchange (defined as > 5% change in exchange, > 0.4 Da mass difference in exchange, a *p*-value < 0.01 using a two-tailed Student's *t*-test). Each point represents an individual peptide, with those colored in red having a significant difference, with error bars showing standard deviation (n=3). Liposomes were generated with **(E)** 60 mol% 4ME-PC, 20 mol% 4ME-PE and 20 mol% 4ME-PA, **(F)** 80 mol% 4ME-PC, 20 mol% 4ME-PE or **(G)** 60 mol% DOPC, 20 mol% DOPE and 20 mol% DAG. A map of deuterium exchange rate according to all peptides throughout the entire PLIN3 was generated based on the alphaFold predicted PLIN3 structure and color coded according to the legend. The full set of peptides is shown in the source data.

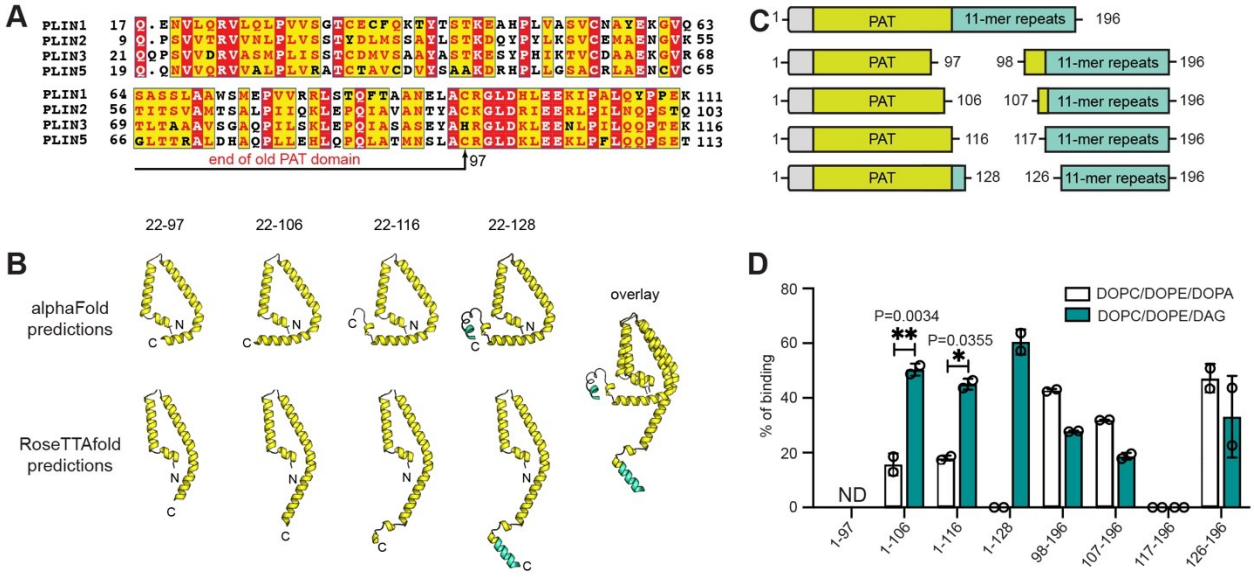

Figure 3. An expanded PAT domain binds DAG enriched membranes

A) Multiple sequence alignment of the N-terminus of human PLIN 1,2,3 and 5. The previously suggested PAT domain (residues 1-97) is indicated with black arrow.

B) Putative PAT domain triangular structures predicted by both alphaFold and RoseTTAfold.

C) Schematic of PAT domain constructs and the counterpart 11-mer repeats constructs.

D) Quantitative analysis of liposome recruitment for various PAT domain and 11-mer repeats constructs. Statistical analysis for quantification of liposome binding was performed using twoway ANOVA with Tukey's multiple comparison test (n=2).

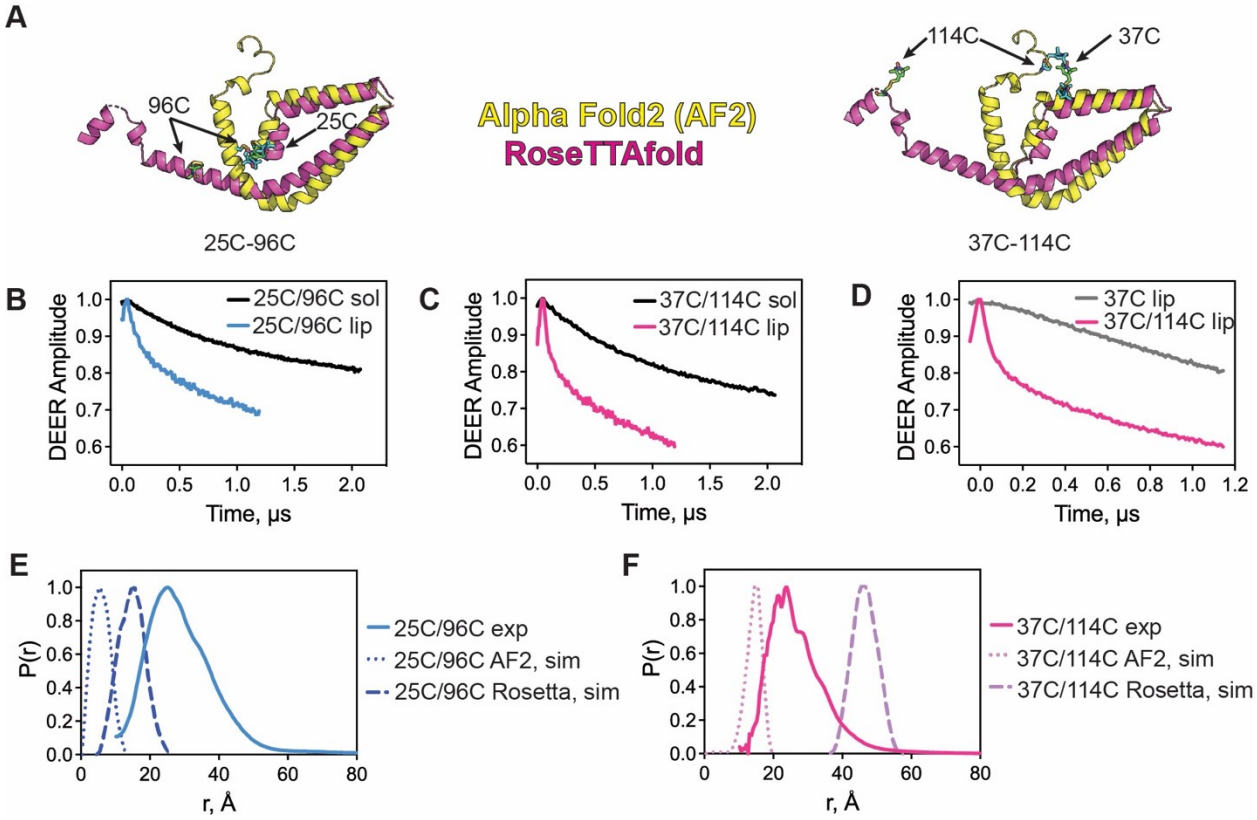

Figure 4. Membrane-induced conformational rearrangements are consistent with a PAT domain tertiary structure

A) Cartoon representation of the PAT domain structure predicted by AlphaFold2 (yellow) and RoseTTAFold (magenta). The position of the spin-labeled residues are highlighted. **B, C)** Time domain signals from DEER spectroscopy of double-labeled **(B)** 25C/96C and **(C)** 37C/114C in solution (sol) and on liposomes (lip).

D) Time domain signals from DEER spectroscopy of double-labeled 37C/114C and singlelabeled 37C proteins on liposomes.

E, F) Distance distributions from DEER spectroscopy of **(E)** 25C/96C and **(F)** 37C/114C determined experimentally (exp) and from MtsslWizard simulations using the AlphaFold2 (AF2, sim) and RoseTTaFold (Rosetta, sim) predicted structures.

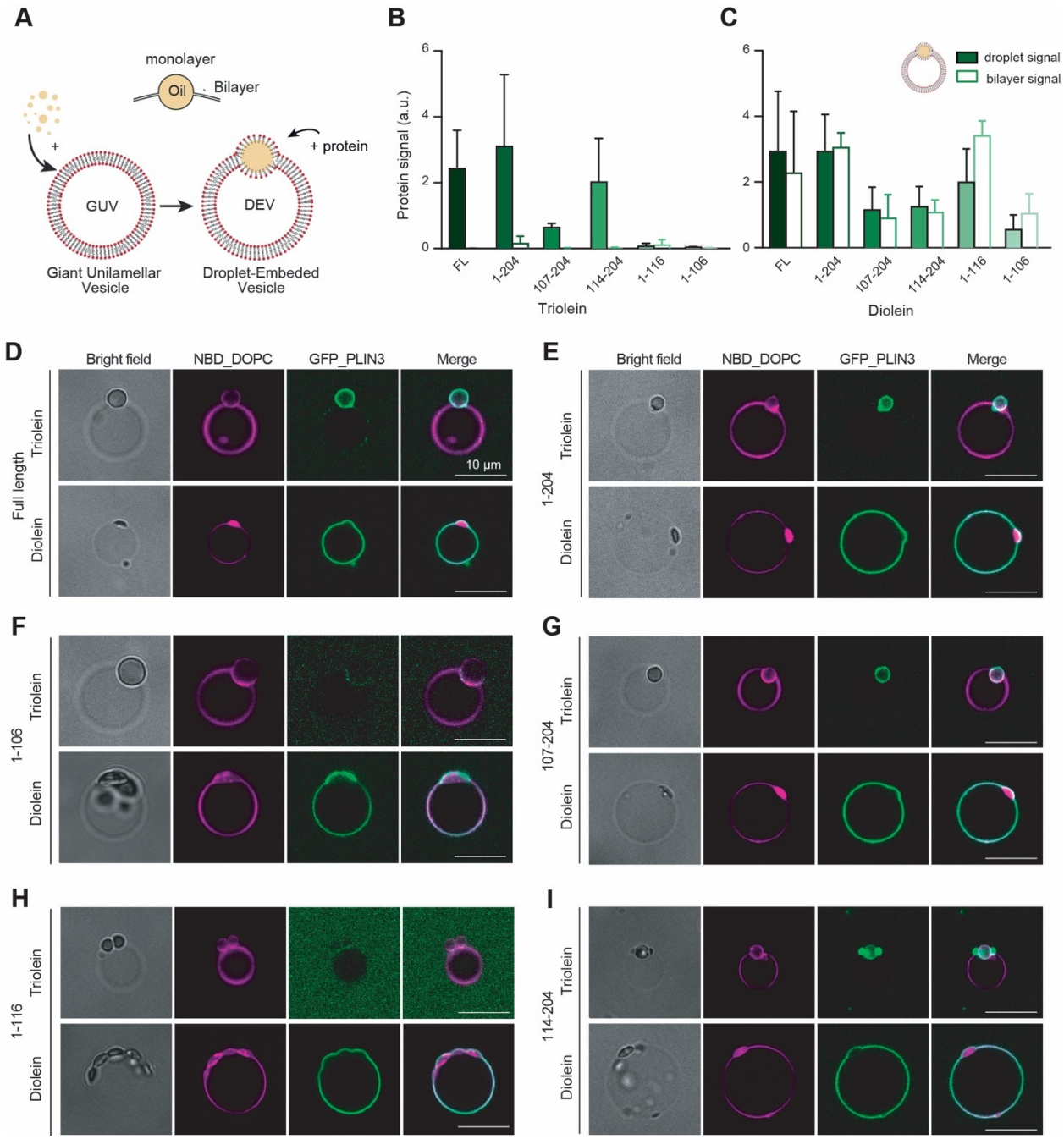

Figure 5. **DAG recruits PLIN3 to membrane bilayers and LD droplets in vitro**

A) A diagram of generation of DEVs by mixing oils and giant unilamellar vesicles (GUVs). **B, C)** Quantification of the recruitment of GFP tagged PLIN3 constructs to droplet embedded vesicles (DEVs) containing (B) triolein or (C) Diolein**.** Statistical analysis was done with a Mann– Whitney non-parametric test. P<0.01 for all proteins. Three different experiments were performed and 10 to 15 DEVs quantified for each experiment.

D-I) Fluorescent microscopic images of N-terminal GFP tagged full length and PLIN3 constructs (green) comprised of PAT domain and 11-mer repeats to (DEVs) (magenta) that are generated with fluorescent labeled phospholipids and oils. F) and H) Recruitment of PAT domain constructs. Almost no recruitment of PAT domain constructs in the presence of Triolein. G) and I) Recruitment of 11-mer repeats constructs.

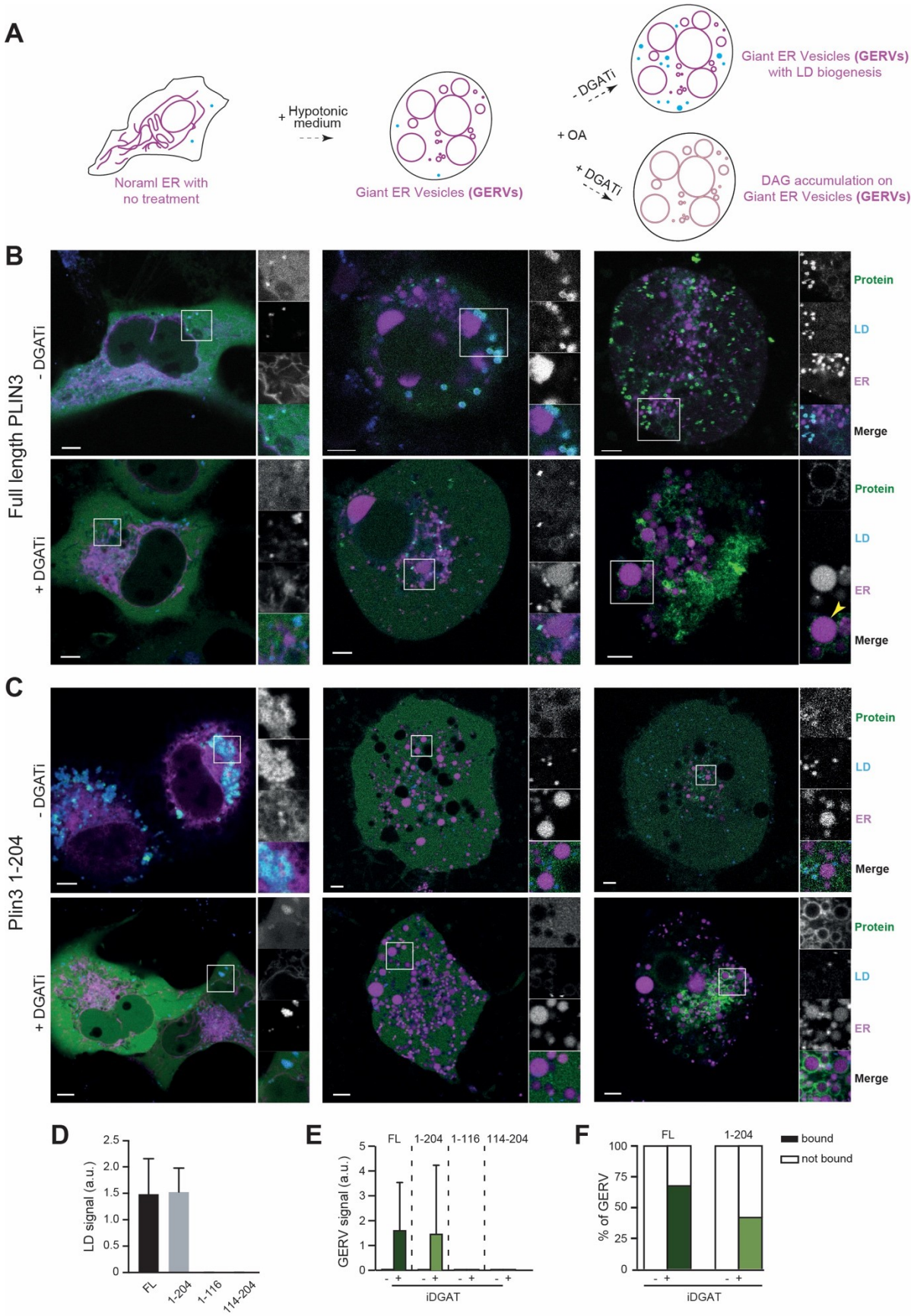
A
Noraml ER with no treatment
+ Hypotonic medium
Giant ER Vesicles (GERVs)
- DGATi
Giant ER Vesicles (GERVs) with LD biogenesis
+ OA
+ DGATi
DAG accumulation on Giant ER Vesicles (GERVs)
B
Full length PLIN3
- DGATi
+ DGATi
Protein
LD
ER
Merge
C
Plin3 1-204
- DGATi
+ DGATi
Protein
LD
ER
Merge
D
LD signal (a.u.)
FL
1-204
1-116
114-204
E
GERV signal (a.u.)
FL
1-204
1-116
114-204
iDGAT
F
% of GERV
FL
1-204
bound
not bound
iDGAT

Figure 6. Both PAT domain and 11-mer repeats are necessary for PLIN3 recruitment to DAG enriched ER membranes in Cos7 cells

A) A diagram of treatment of Giant ER Vesicle formation and treatment of oleic acid and DGATi to induce DAG accumulation on the ER in Cos7 cells.

B, C) Subcellular localization of GFP tagged full length PLIN3 and PAT/11-mer repeats (1-204) were visualized in green in Cos7 cells under fluorescent microscope ZEISS LSM800 Airyscan. ER was visualized with ER specific marker RFP-KDEL in magenta. Lipid droplets were labeled with LipidTox Deepred to stain neutral lipids in cyan. After treated with hypotonic medium, cells were supplemented with oleate in the presence or absence of DGAT1/2 inhibitors. Each experiment was performed more than 3 times.

D) Quantification of the amount of various PLIN3 constructs on LDs

E) Quantification of the amount of various PLIN3 constructs on GERV after oleate treatment in the presence and the absence of DGAT1/2 inhibitors.

F) % of GERV that are covered with full length PLIN3 or PAT/11-mer repeats construct (1-204) after oleate treatment in the presence and the absence of DGAT1/2 inhibitors.

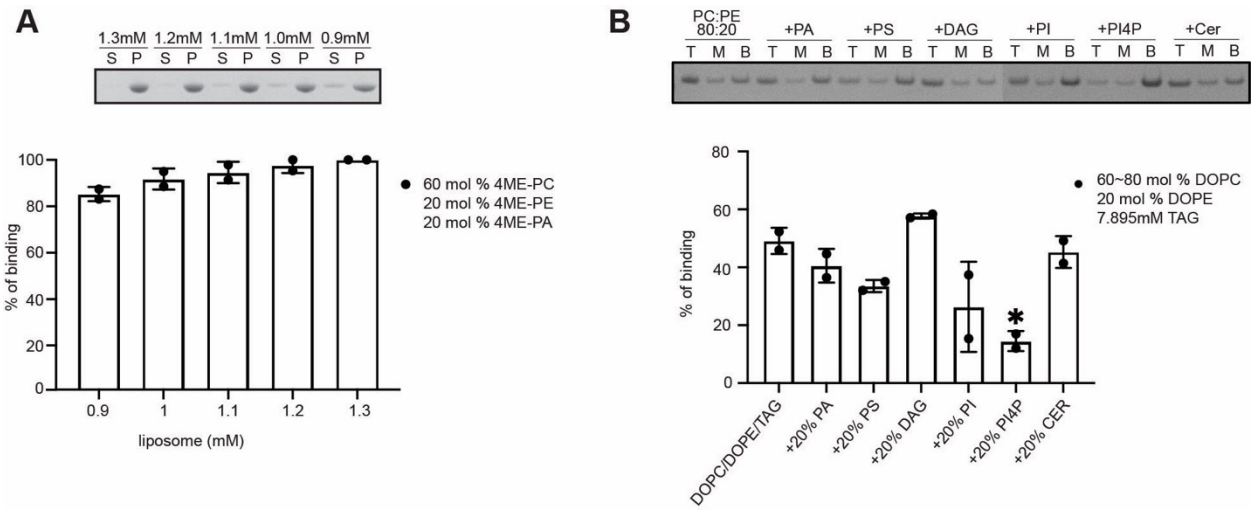

Supplementary Figure 1.

A) SDS-PAGE and quantitative analysis of human PLIN3 recruitment by increasing the total amount of liposomes. The molar ratio of 4ME-PC/4ME-PE/4ME-PA in 60:20:20 was kept same. Lane S represents unbound human PLIN3 from supernatant. Lane P represents pelleted human PLIN3 that bound to liposomes. Bar graph shows total increase in liposome amount results almost 100% recruitment of PLIN3 to liposome.

A) SDS-PAGE and Quantitative analysis of human PLIN3 recruitment to ALDs generated with DO-phospholipids and TAGs (C16) by adding additional with 20 mol% of lipids such as PS, PA, DAG, PI, PI4P and ceramide. Top, middle and bottom fractions after sucrose-gradient centrifuge were indicated as T, M and B, respectively. Statistical analysis was performed using ordinary one-way ANOVA with Tukey's multiple comparison test (n=2, *, p=0.0258, ***,p=0.004).

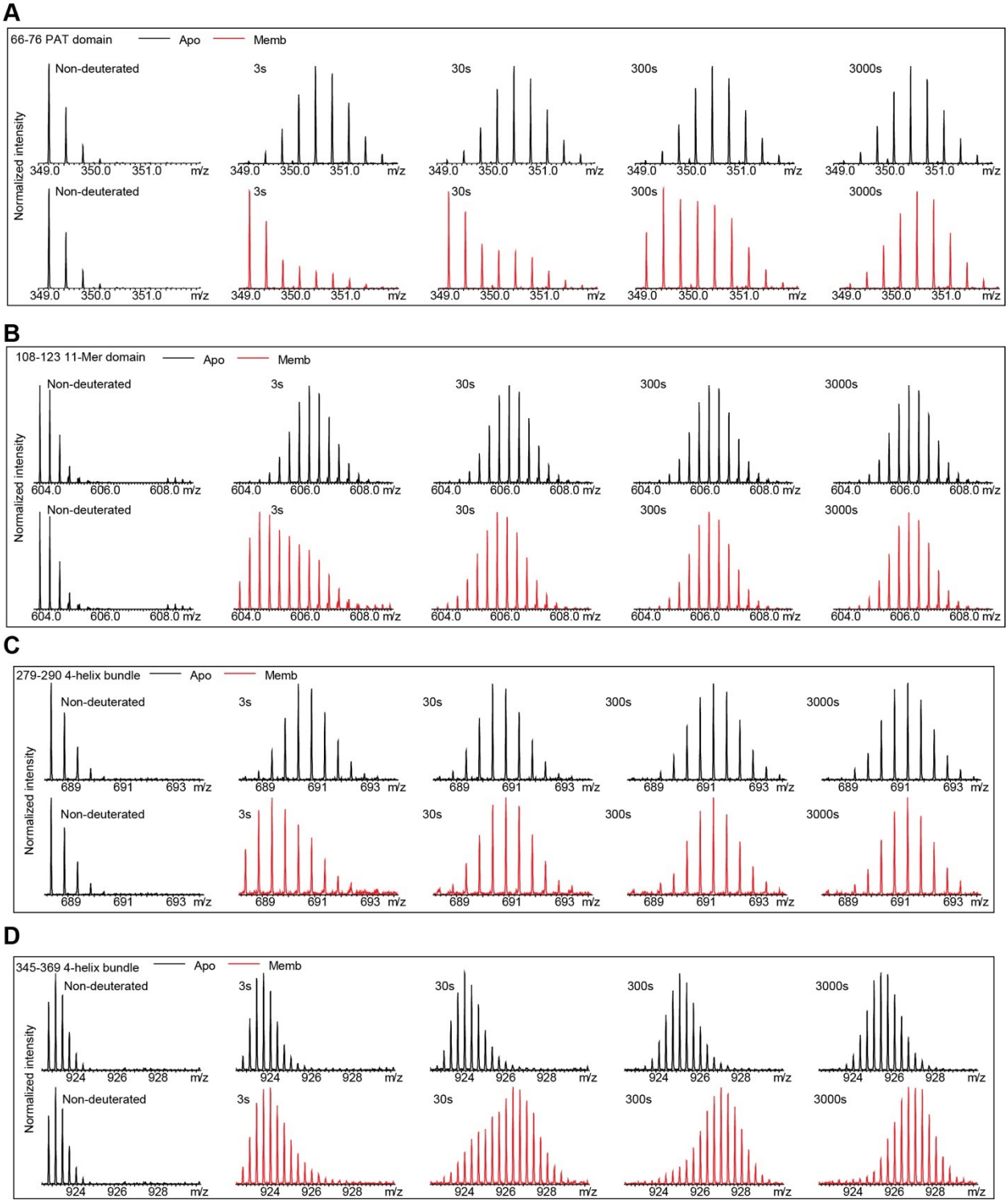
A
66-76 PAT domain
Apo
Memb
Non-deuterated
3s
30s
300s
3000s
Normalized intensity
349.0
350.0
351.0
m/z
B
108-123 11-Mer domain
604.0
606.0
608.0 m/z
C
279-290 4-helix bundle
689
691
693 m/z
D
345-369 4-helix bundle
924
926
928 m/z

Supplementary Figure 2.
Representative bimodal distribution mass spectra from the peptides at PAT domain, 11-mer repeats, and 4-helix bundle of PLIN3 after deuterium exchange.

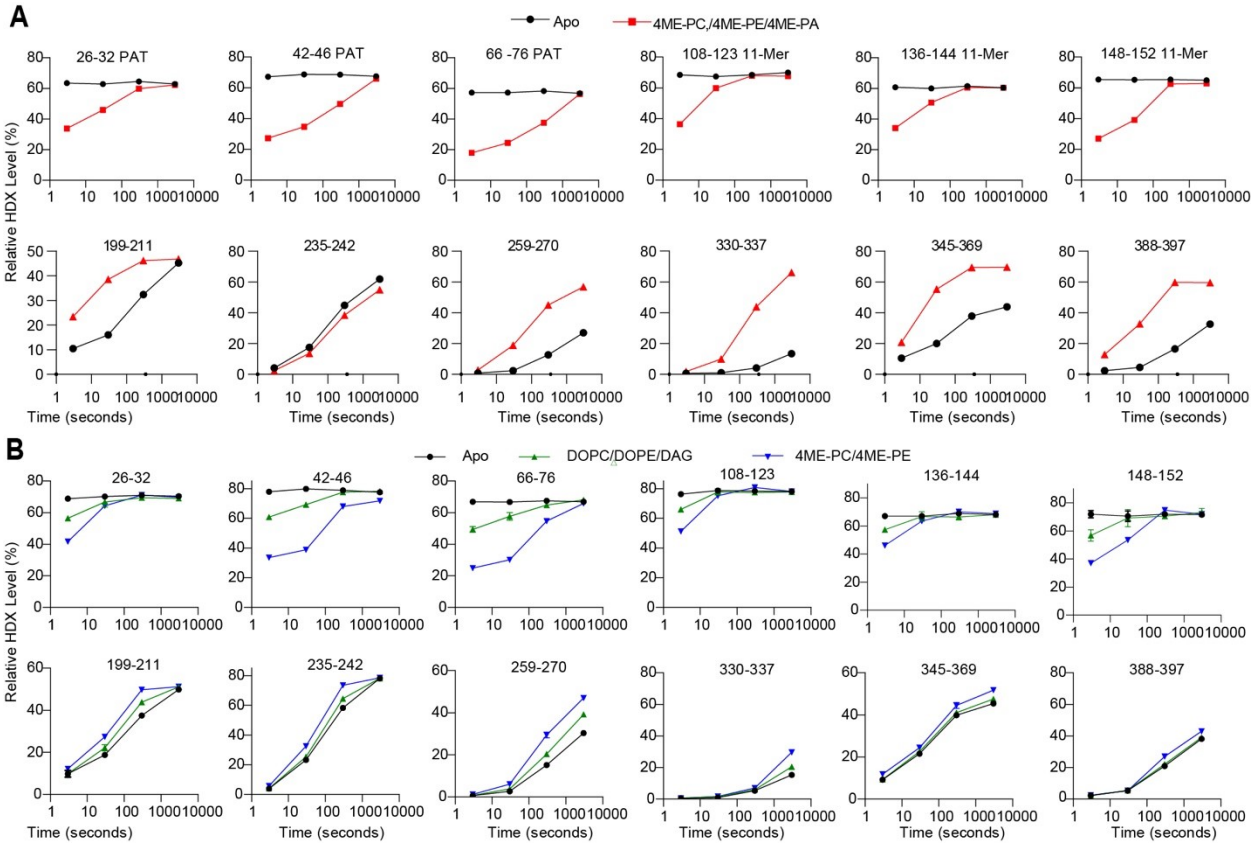

Supplementary Figure 3.

A) Deuterium exchange uptake plots for selected peptides in the PAT domain, 11-mer repeats and 4-helix bundle were plotted across all timepoints as 3s, 30s, 300s and 3000s. Data points in the absence and presence of liposomes were colored in black and red, respectively. Liposomes were generated with 60 mol% 4ME-PC, 20 mol% 4ME-PE and 20 mol% 4ME-PA). All peptides are shown in the source data.

B) Deuterium exchange uptake plots for selected peptides in the presence of two different liposomes are plotted across all timepoints as 3s, 30s, 300s and 3000s colored according the the legend. All peptides are shown in the source data.

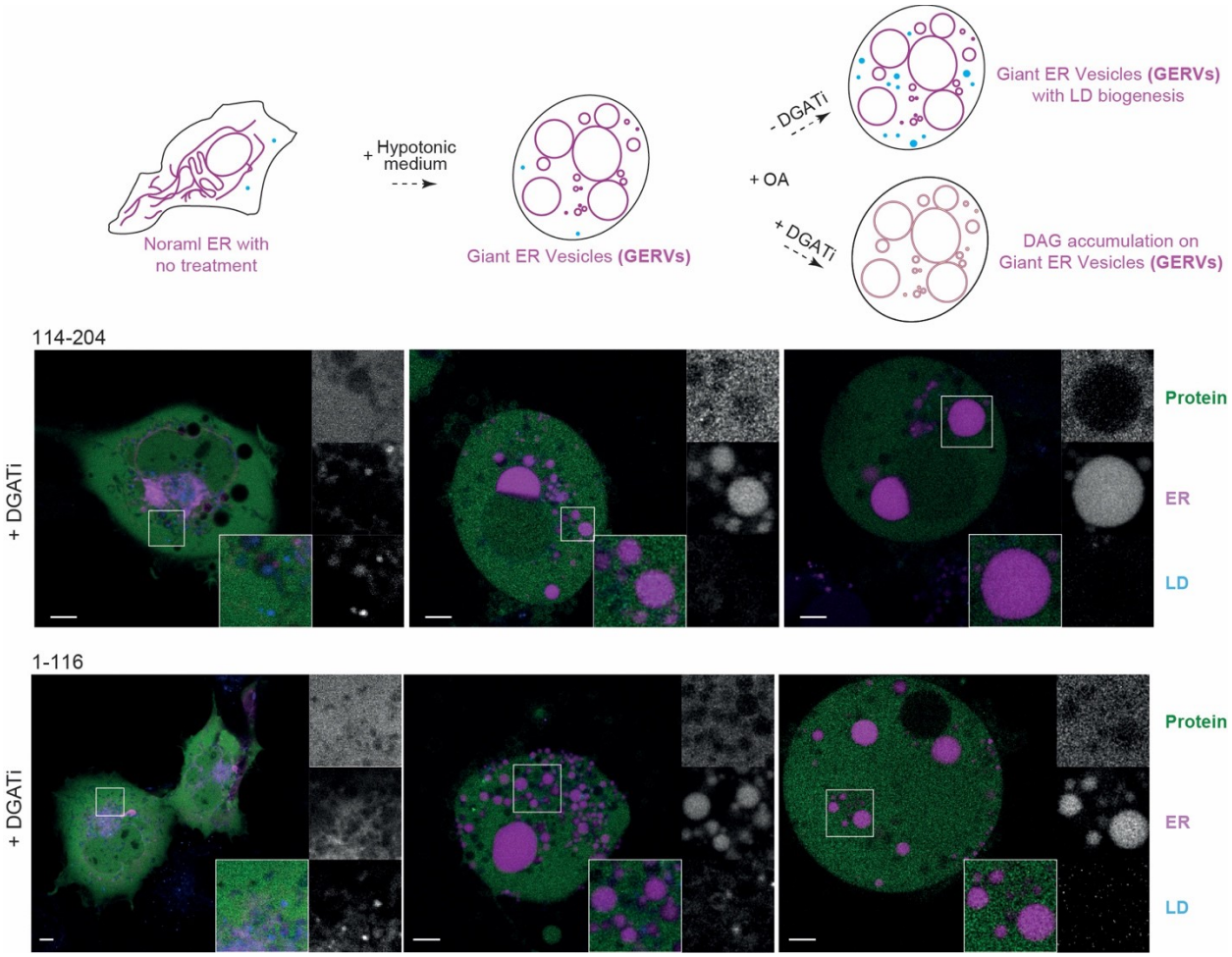

Supplementary Figure 4.
Subcellular localization of GFP tagged 114-204 and 1-116 constructs of PLIN3 was visualized in green in Cos7 cells under fluorescent microscope ZEISS LSM800 Airyscan. ER was visualized with ER specific marker RFP-KDEL in magenta. Lipid droplets were labeled with LipidTox Deepred to stain neutral lipids in cyan. After treated with hypotonic medium, cells were supplemented with oleate in the presence or absence of DGAT1/2 inhibitors.

Supplementary Table 1.
Summary of all HDX-MS data processing.

Data set	PLIN3 order disorder Expt-1	PLIN3 Apo Expt-2	PLIN3 + 60% 4ME-PC, 20% 4ME-PE, 20% 4ME-PA liposomes Expt-2	PLIN3 Apo Expt-3	PLIN3 + 60% DOPC, 20% DOPE, 20% DAG liposomes Expt-3	PLIN3+ + 80% 4ME-PC, 20% 4ME-PE liposomes Expt-3
HDX reaction details	%D_2O=84.9 % $pH_{(read)}$=7.5 Temp=18ºC	%D_2O=72% pH(read)=7.5 Temp=18ºC	%D_2O=72% pH(read)=7.5 Temp=18ºC	%D_2O=72% $pH_{(read)}$=7.5 Temp=18ºC	%D_2O=72% $pH_{(read)}$=7.5 Temp=18ºC	%D_2O=72% $pH_{(read)}$=7.5 Temp=18ºC
HDX time course (seconds)	0.3s, fully deuterated	3s, 30s, 300s, 3000s	3s, 30s, 300s, 3000s	3s, 30s, 300s, 3000s	3s, 30s, 300s, 3000s	3s, 30s, 300s, 3000s
HDX controls	N/A	N/A	N/A	N/A	N/A	N/A
Backexchange	Corrected by fully deuterated sample	No correction, deuterium levels are relative	No correction, deuterium levels are relative	No correction, deuterium levels are relative	No correction, deuterium levels are relative	No correction, deuterium levels are relative
Number of peptides	144	90	90	90	90	90
Sequence coverage	99.8%	91.7%	91.7%	91.7%	91.7%	91.7%
Average peptide /redundancy	Length= 17.3 Redundancy = 5.4	Length= 13.0 Redundancy = 2.6	Length= 13.0 Redundancy = 2.6	Length= 13.0 Redundancy = 2.6	Length= 13.0 Redundancy = 2.6	Length= 13.0 Redundancy = 2.6
Replicates	3	3	3 Average StDev=0.6%	3	3	3
Repeatability	Average StDev=0.4%	Average StDev=0.6%		Average StDev=0.8%	Average StDev=1.0%	Average StDev=0.9%
Significant differences in HDX	N/A	>5% and >0.4 Da and unpaired ttest ≤0.01	>5% and >0.4 Da and unpaired ttest ≤0.01	>5% and >0.4 Da and unpaired ttest ≤0.01	>5% and >0.4 Da and unpaired ttest ≤0.01	>5% and >0.4 Da and unpaired ttest ≤0.01